Influence of diurnal heating on stratification and residual circulation of Georges Bank

Changsheng Chen,[1] Robert C. Beardsley,[2] Peter J. S. Franks,[3] and J. Van Keuren[4]

Received 4 December 2001; revised 26 April 2003; accepted 13 May 2003; published 22 November 2003.

[1] The influence of the diurnal heat flux on summer stratification and residual circulation over Georges Bank was examined using a three-dimensional primitive equation numerical circulation model. For a given spatially uniform and time-varying heat flux the model results show that the surface water is heated much faster on the southern flank than on the northern flank and much faster in the stratified region than in the mixed region. Heating significantly strengthens the tidal mixing front and intensifies the frontward convergence near the surface. As seasonal stratification develops, the location of the tidal mixing front gradually shifts on bank on the southern flank, while remaining almost unchanged on the northern flank. Response of the tidal currents to the diurnal variation in the heat flux varies across Georges Bank. It changes periodically with tidal cycles on the southern flank but is locked to the phase of the eastward tidal current on the northern flank. This phase-lock feature directly contributes to the intensification of the along-bank residual current jet on the northern flank. Diagnostic analysis suggests that this intensification is mainly caused by the heat-enhanced, cross-bank momentum flux. Model-computed variations of near-surface temperature and residual currents are in good agreement with satellite-derived sea surface temperature data and drifter measurements. *INDEX TERMS:* 4219 Oceanography: General: Continental shelf processes; 4227 Oceanography: General: Diurnal, seasonal, and annual cycles; 4255 Oceanography: General: Numerical modeling; 4279 Oceanography: General: Upwelling and convergences; 4528 Oceanography: Physical: Fronts and jets; *KEYWORDS:* heat flux, tidal mixing front, residual current, stratification, frontward convergence

Citation: Chen, C., R. C. Beardsley, P. J. S. Franks, and J. Van Keuren, Influence of diurnal heating on stratification and residual circulation of Georges Bank, *J. Geophys. Res.*, *108*(C11), 8008, doi:10.1029/2001JC001245, 2003.

1. Introduction

[2] Moored measurements made during the 1995–1999 U.S. Global Ocean Ecosystems Dynamics (GLOBEC) Northeast Atlantic/Georges Bank (GB) Program (Figure 1) show that strong seasonal changes in the surface heat flux and wind forcing help drive pronounced cycles of stratification and mixing over GB [*Lentz et al.*, 2003; *Beardsley et al.*, 2003]. In winter, cooling-induced convection and tidal mixing forms a vertically well-mixed water column over the whole bank. During spring and summer, decreasing wind mixing and increasing solar heating cause a strong increase in stratification on the southern flank, leading to an on-bank movement of the tidal mixing front. This on-bank migration of the tidal mixing front is much less apparent on the northern flank, even though stratification also increases there because of surface heating.

[3] Heat flux and wind stress variability directly influence the seasonal pattern of residual circulation over GB. An example can be seen in recent Lagrangian measurements made with satellite-tracked drifters [*Limeburner and Beardsley*, 1996; *Brink et al.*, 2003]. During summer, drifters moved clockwise around the bank, with a narrow path in the tidal mixing frontal zone on the southern and northern flanks and three distinct trajectory patterns on the northeastern side of the bank. As storms increase in intensity in fall, the drifter tracks become open, and drifters quickly leave the bank. The summer intensification of the clockwise residual circulation around GB is believed to be due to a combination of the seasonal development of the tidal mixing front, nonlinear interaction of internal waves near the fronts, and modification of internal friction [*Loder and Wright*, 1985; *Chen*, 1992; *Naimie et al.*, 1994; *Chen and Beardsley*, 1995; *Chen et al.*, 1995a; *Naimie*, 1996]. These physical processes are all closely related to the seasonal development of stratification, which is thought to be due to the local surface heat flux [*Mountain et al.*, 1996], the flow of low-salinity water across the Great South and Northeast Channels to GB [*Chen et al.*, 1995b; *Smith*, 1983, 1989], and on-bank intrusion of slope water associated with warm-core rings [*Brooks*, 1987; *Garfield and Evans*, 1987].

[1]School for Marine Science and Technology, University of Massachusetts Dartmouth, New Bedford, Massachusetts, USA.
[2]Department of Physical Oceanography, Woods Hole Oceanographic Institution, Woods Hole, Massachusetts, USA.
[3]Integrative Oceanography Division, Scripps Institution of Oceanography, University of California, San Diego, La Jolla, California, USA.
[4]Department of Biology, Woods Hole Oceanographic Institution, Woods Hole, Massachusetts, USA.

0148-0227/03/2001JC001245$09.00

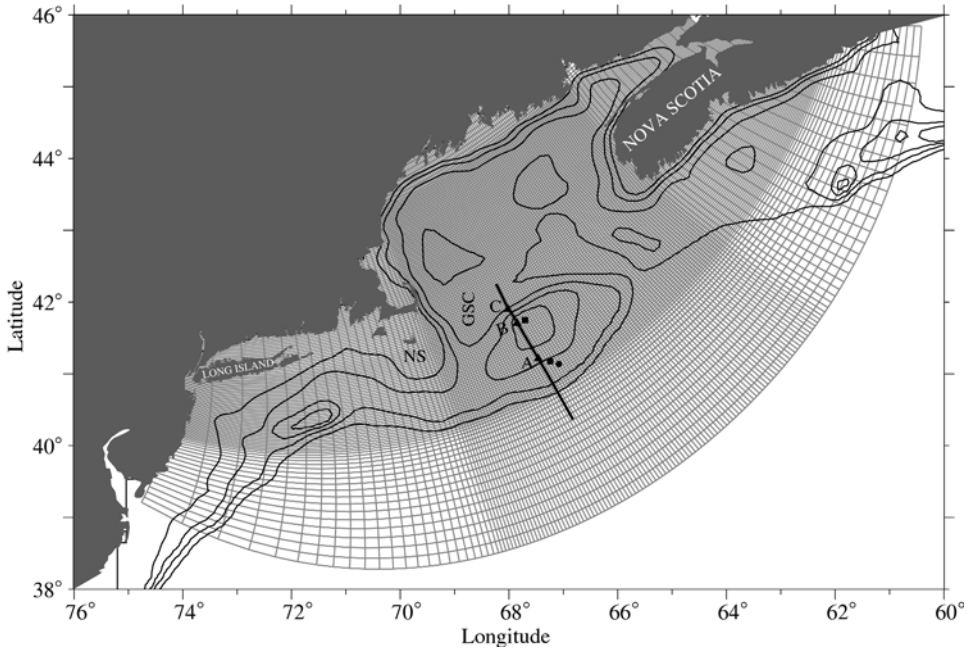

Figure 1. Bathymetry of New England continental margin with numerical model grid overlaid. The 40, 60, 100, and 200 m isobaths are shown. The bold NW/SE line across Georges Bank (GB) is the section used to present the cross-bank distribution of temperature and currents. The triangles are selected sites on the section. The circle is the location of the ST1 meteorological buoy that collected data for estimation of the surface heat flux. Squares are selected sites for model comparison with satellite-derived SST. GSC is Great South Channel; NS is Nantucket Shoals.

[4] The surface heat flux in summer is dominated by shortwave insolation, so that the net flux exhibits a large diurnal variation, from near 0 at night to a clear-sky maximum of over 900 W/m^2 near noon (Figures 2 and 3) [*Beardsley et al.*, 2003]. During July 1995, for example, the monthly mean daytime maximum was 748 W/m^2, resulting in a monthly mean net flux of 247 W/m^2. Our current understanding of the role of this large diurnal heating cycle on the stratification and circulation on GB is quite limited. Using moored data collected in the 1995 GLOBEC GB program, *Lentz et al.* [2003] has shown that the mean net surface flux accounts for most of the local change in depth-integrated heat content on the southern flank; however, little is known about internal heating in the water column due to the penetration and absorption of the dominant shortwave component and about how this might effect the tidal residual circulation in the tidally dominated GB region.

[5] The objective of this paper is to investigate the response of stratification and flow over GB to the large diurnal heat flux. A series of idealized numerical circulation model experiments were conducted starting with summer stratification and tidal forcing and then adding the surface heat flux using different models for shortwave penetration. The results from these experiments allow us to examine the sensitivities of the model temperature field and residual circulation to the different penetration models and to develop a better idea of how best to represent the surface heat flux in model experiments with more realistic surface forcing. In section 2 the circulation model and shortwave penetration model are introduced. In section 3 the

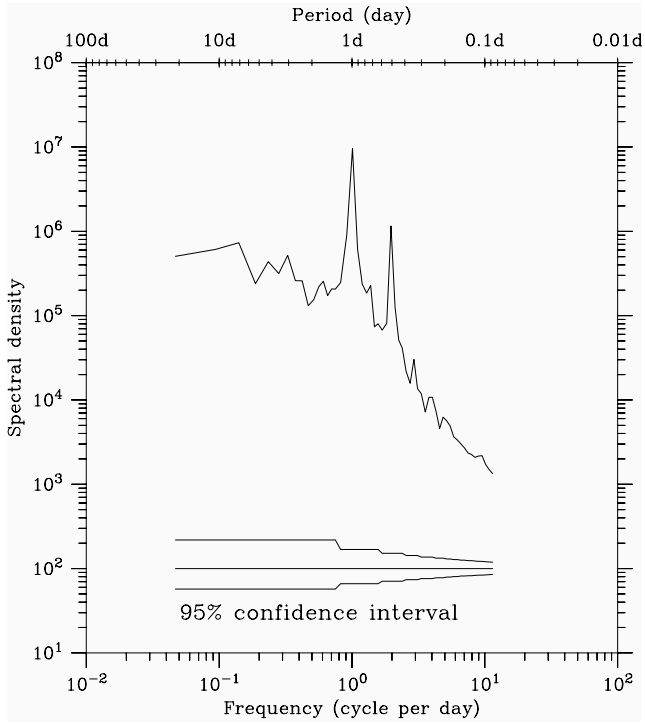

Figure 2. Net surface heat flux spectrum for hourly data collected February–August 1995 at ST1 on the southern flank of Georges Bank. Units are (W/m^2)^2/cpd. ST1 was located at 67°33.5′W, 40°51.9′N (circle in Figure 1). Figure 2 was plotted using data from *Beardsley et al.* [2003].

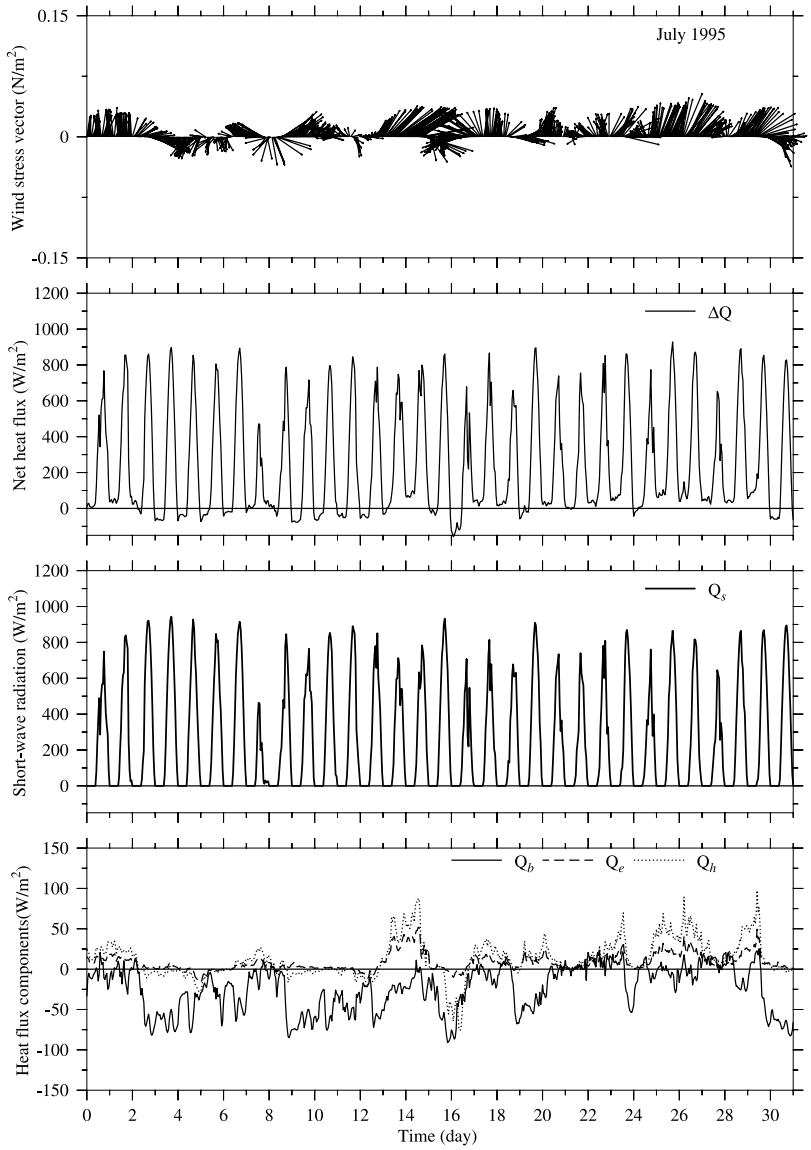

Figure 3. Time series of surface wind stress (N/m^2), net heat flux (Q_n), and shortwave (Q_s), longwave (Q_b), latent (Q_e), and sensible (Q_h) heat flux components at ST1 during July 1995. Figure 3 was plotted using data from *Beardsley et al.* [2003].

model results for different penetration parameters are described, and the model surface temperatures are compared with satellite-derived sea surface temperatures (SSTs). In section 4, physical processes contributing to the summertime intensification of the residual current jet are discussed. A summary is given in section 5.

2. Design of Numerical Experiments

[6] The numerical model used in this study is a modified version of the three-dimensional coastal ocean circulation model (called ECOM-si) developed originally by *Blumberg and Mellor* [1987]. This model incorporates the modified Mellor and Yamada level 2.5 turbulent closure scheme to provide a time- and space-dependent parameterization of vertical turbulent mixing [*Mellor and Yamada*, 1974, 1982; *Galperin et al.*, 1988]. The original *Blumberg and Mellor* [1987] model (called the Princeton Ocean Model) is a time-splitting model in which the flow is divided into barotropic and baroclinic modes and numerical equations for these two modes are solved using two distinct time steps. ECOM-si is solved following a semi-implicit numerical method. This method treats the barotropic pressure gradient in the momentum equations and the velocity convergence in the continuity equation implicitly, and thus the governing equations can be solved using a single time step [*Casulli*, 1990]. This approach improves model efficiency and accuracy while reducing unbalanced heat gain/loss during long simulations.

[7] A detailed description of the configuration of ECOM-si used here was given by *Chen et al.* [2001]. The model domain covers the entire Gulf of Maine (GOM)/GB region and is enclosed by an open boundary running from the New Jersey shelf to the Nova Scotia shelf (Figure 1). The model grid utilizes orthogonal curvilinear coordinates in the horizontal

and a σ-coordinate transformation in the vertical. The horizontal resolution varies from 2.5 to 4 km over GB and in the interior region of the GOM and 4 to 20 km near the open boundary. Forty-one σ levels with a nonuniform interval are specified in the vertical, which correspond to a vertical resolution of 0.04 to 0.2 m on the 40-m isobath over GB and adjacent shelf regions and about 0.3 m in the upper 10 m on the 300-m isobath. The bottom depth at each model grid point is interpolated directly from the high-resolution U.S. Geological Survey bathymetric database provided by E. Roworth and R. Signell. To avoid the σ-coordinate error over the very steep continental slope, the water depth off the southern shelf break of GB is made at a uniform 300 m. The model time step is 414 s, which results in 108 time steps over a M_2 tidal cycle.

[8] The model is forced initially by the barotropic M_2 tidal elevation and phase at the open boundary, using values interpolated from the *Egbert et al.* [1994] global $0.5^\circ \times 0.5^\circ$ inverse tidal model. A gravity wave radiation condition on current is specified at the open boundary to minimize the reflection of wave energy into the computational domain [*Chen and Beardsley*, 1995]. The model is run as an initial value problem with early summer stratification. The initial temperature distribution is specified by a linear function of z, with a value of 15°C at the surface and 6°C at the bottom (at depth 300 m). To simplify the model problem and focus on physical processes associated with the tidal mixing front, salinity is set to a constant value of 35 practical salinity units everywhere in the model domain, making density depend solely on temperature.

[9] The surface heat flux is added in the model run after the stratified tidal rectified current reaches a quasi-equilibrium state after 10 model days. To examine the influence of diurnal heating on intensification of stratification and residual circulation over GB in summer, we take a typical clear-sky diurnal cycle of the heat flux observed on the southern flank in late June and early July 1995 as the model flux (Figure 4). The model flux has a maximum of 800 W/m^2 and minimum of -70 W/m^2, respectively, with a daily averaged net heat input of about 365 W/m^2. While this value is larger than the June or July 1995 monthly mean net flux of about 250 W/m^2 because of intermittent cloudiness [*Beardsley et al.*, 2003], it approximates the surface heat flux for a period with rapid increase in satellite-derived SST recorded in late June 1995. The SST data used in the model-data comparison were taken on 21 June through 11 July 1995.

[10] The net surface net heat flux $Q_n(t)$ consists of four components: shortwave, longwave, sensible, and latent fluxes. Here the longwave, sensible, and latent fluxes are assumed to occur at the ocean surface, while the net downward shortwave flux has a vertical structure approximated by

$$\mathrm{SW}(z,t) = \mathrm{SW}(0,t)\left[\mathrm{Re}^{\frac{z}{a}} + (1-R)e^{\frac{z}{b}}\right], \qquad (1)$$

where SW(0,t) is the net shortwave flux at the sea surface, a and b are the attenuation lengths for longer and shorter (blue-green) wavelength shortwave components, and R is the percent of the total shortwave flux associated with the longer-wavelength component. This profile was first

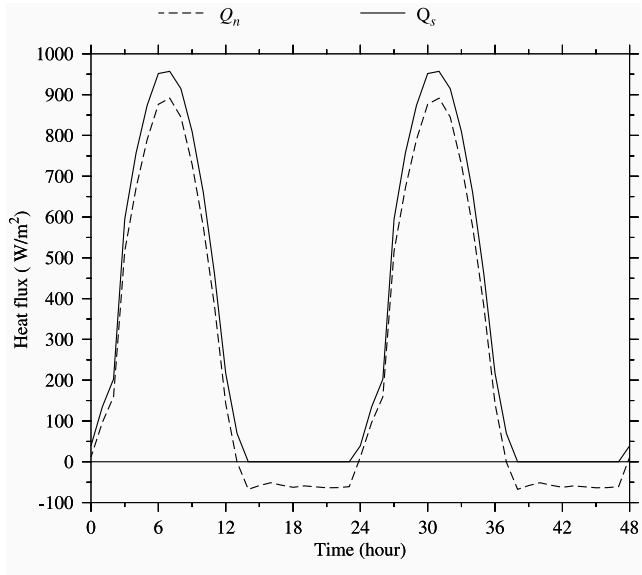

Figure 4. Model input heat flux. Q_n is the net heat flux at the surface, and Q_s is the shortwave component.

suggested by *Kraus* [1972] and was used in numerical studies of diurnal heating in the open ocean by *Simpson and Dickey* [1981a, 1981b]. Here we treat the absorption of the downward flux as a "body force" H in the temperature (heat) equation in the form of

$$\hat{H}(z,t) = \frac{\partial \mathrm{SW}(z,t)}{\partial z} = \frac{\mathrm{SW}(0,t)}{\rho_o c_p}\left[\frac{R}{a}e^{\frac{z}{a}} + \frac{1-R}{b}e^{\frac{z}{b}}\right], \qquad (2)$$

where ρ_o and c_p are the reference density and specific heat of sea water. Compared with the "traditional" flux formulation based on a monotonic exponential decay of shortwave radiation with depth, this approach provides a more accurate prediction of the near-surface temperature [*Kraus*, 1972].

[11] The resulting surface boundary condition for temperature is then

$$\left.\frac{\partial T}{\partial z}\right|_{z=\zeta} = \frac{1}{\rho_o c_p K_h}[Q_n(t) - \mathrm{SW}(0,t)], \qquad (3)$$

where T is temperature, ζ is the surface elevation, and K_h is the thermal diffusion atthe surface. *Paulson and Simpson* [1977] estimated values of the three parameters R, a, and b for different water types. For type III "coastal" water they suggested that $R = 0.78$, $a = 1.4$ m, and $b = 7.9$ m. Analysis of in situ profile measurements of photosynthetically active radiation (PAR) made on GB during May–June 1995 (Appendix A) suggests that $b = 6.3 \pm 0.7$ m, with no significant difference between the well-mixed and stratified regions over GB. With no GB data available to estimate R and a directly, we use here the *Paulson and Simpson* [1977] type III "coastal" R and a values with our estimate for b as the basic radiation parameter set for our model study. As noted next, several experiments were also conducted with different values of these parameters to examine model sensitivity.

[12] Numerical experiments were conducted with the following radiation parameter sets. For case A, $R = 0.78$, $a = 1.4$ m, and $b = 6.3$ m, basic two-component heating, and our best estimate of realistic values for GB during July 1995. For case B, $R = a = b = 0$ and surface heating only, with all heat being absorbed in the top model grid cells. For case C, $R = 1$, $a = 10$ m, and $b = 0$ m, corresponding to deeper single-component heating. For case D, ''coastal/open ocean'' heating, $R = 0.78$, $a = 1.4$ m, and $b = 7.9$ m in the mixed region on GB (the *Paulson and Simpson* [1977] type III values) and $R = 0.58$, $a = 0.35$ m, and $b = 23$ m in the stratified region, suggested by *Simpson and Dickey* [1981a, 1981b] as representative of ''blue'' ocean water.

[13] The model results will be compared with satellite-derived SST data. Daily averaged SST values are first made from the 5-day optimally interpolated SST analysis produced by J. Bisagni (http://www.smast.umassd.edu). A 5-point average around selected model comparison sites is then made with the SST gridded data to match the geometric locations of the SST and model output.

3. Model Results

3.1. Tidal Mixing Fronts and Residual Circulation

[14] To better understand the influence of the diurnal heat flux on summer stratification and residual circulation over GB, a brief summary of the model results for the base case with only tidal forcing is provided here first [*Chen et al.*, 2001]. In this case the model reproduces the well-defined tidal mixing fronts around GB and Brown Bank and over the Nantucket Shoal (NS) (Figure 5a). Over GB the front is characterized by a narrow zone near the 40-m isobath on the northern flank, between 60- and 80-m isobaths on the northeast flank, and between the 50- and 60-m isobaths on the southern flank. Over NS a well-defined tidal mixing front is located along the 60-m isobath with connection to the frontal zone on GB through the Great South Channel (GSC). Cold water bands are found within the frontal zone on the northeastern and southern flanks of GB, NS, and the GSC.

[15] The clockwise residual gyre intensities significantly within the frontal zones. Over GB the residual current speed increases to 25–30 cm/s on the northwestern flank, 15–25 cm/s on the northern flank, and 5–8 cm/s on the southern flank (Figure 5b). On the cross section shown in Figures 6a and 6b the along-bank current is about 16 cm/s. Water on the northern side of GB moves on bank along three primary paths: (1) along the 40-m isobath on the northwestern edge, (2) between the 50- to 60-m isobaths on the northern edge, and (3) along the 100-m isobath on the northeastern flank. Over NS the residual current is southward, with a maximum speed of about 10–15 cm/s.

[16] Cross-frontal secondary circulation varies with the slope of the bottom topography over GB (Figure 6). On the northern flank it is characterized by a bottom-intensified double-cell circulation, with frontward convergence near the surface and divergence near the bottom. The center of the near-surface convergence is located at the axis of the maximum along-bank residual current within the front. On the southern flank the cross-frontal flow exhibits an asymmetric double-cell circulation, with divergence at the edge of the front near the surface and convergence at the top of the bottom mixed layer. Two branches of upwelling are noticeable within the frontal zone: The first is along isopycnals at the top of the bottom mixed layer, and the second is upward along the vertical isotherms at the edge of the front. These two streams of upwelling waters merge near the surface, causing a maximum upward vertical velocity of 0.007 cm/s near 7 m. In addition, the cross-bank secondary current above and below the bottom mixed layer in the stratified region is characterized by multiple circulation cells. These cells are stronger at the shelf break where the bottom is steepest and become weaker as the thickness of bottom mixing layer increases because of strong tidal mixing. The clockwise secondary circulation, seen within the relatively cold zone between 38- and 52-m isobaths, is a result of local mixing over variable bottom topography [see *Chen et al.*, 2001].

3.2. Heating-Induced Intensification of Stratification and Residual Flow

[17] We now add the surface heat flux and examine how different shortwave penetration models influence the stratification and residual flow. The numerical model is integrated in time from the quasi-equilibrium state using one of the shortwave models and the near-surface model temperatures compared with the daily averaged satellite-derived SST trends. In case A (with our best estimates for R, a, and b) the model provides a reasonable warming tendency in both mixed and stratified regions (Figure 7a). The model-computed diurnal temperature variation ranges from 0.2° to 1°C in the mixed region and about 1° to 2°C in the stratified region. In the mixed region the model-computed water temperature increases linearly with time, which is in good agreement with the SST trend. In the stratified region, SST rises rapidly in the first 10 days and then increases gradually over the next 10 days. This temporal variation is captured by the model.

[18] In case B (with surface forcing only) the absorption of the entire heat flux in the top model layer increases the diurnal variation of the water temperature in both mixed and stratified regions (Figure 7b). The maximum diurnal temperature range near the surface can reach 4°C, which is about 1 time larger than that found in case A. In addition, the model driven by surface heating tends to overheat the near-surface water in the stratified region, even though it has little influence in the mixed region.

[19] In case C (with deeper penetration of a single-component flux) the model produces a steady warming trend in good agreement with SST in the mixed region, but it significantly underestimates the trend of SST in the stratified region (Figure 7c). In addition, the model-computed amplitude of the diurnal variation of the near-surface water temperature is significantly smaller than that found in cases A and B.

[20] In case D (with coastal/ocean heating) the model reasonably reproduces the SST warning trend in the mixed region, even though the model-computed amplitude of the diurnal variation of water temperature is much smaller than that found in cases A and B (Figure 7d). In the stratified region, however, the model exhibits little diurnal variation and warms much slower than SST.

[21] These model results for different shortwave penetration parameters suggest the following. In summer the low-

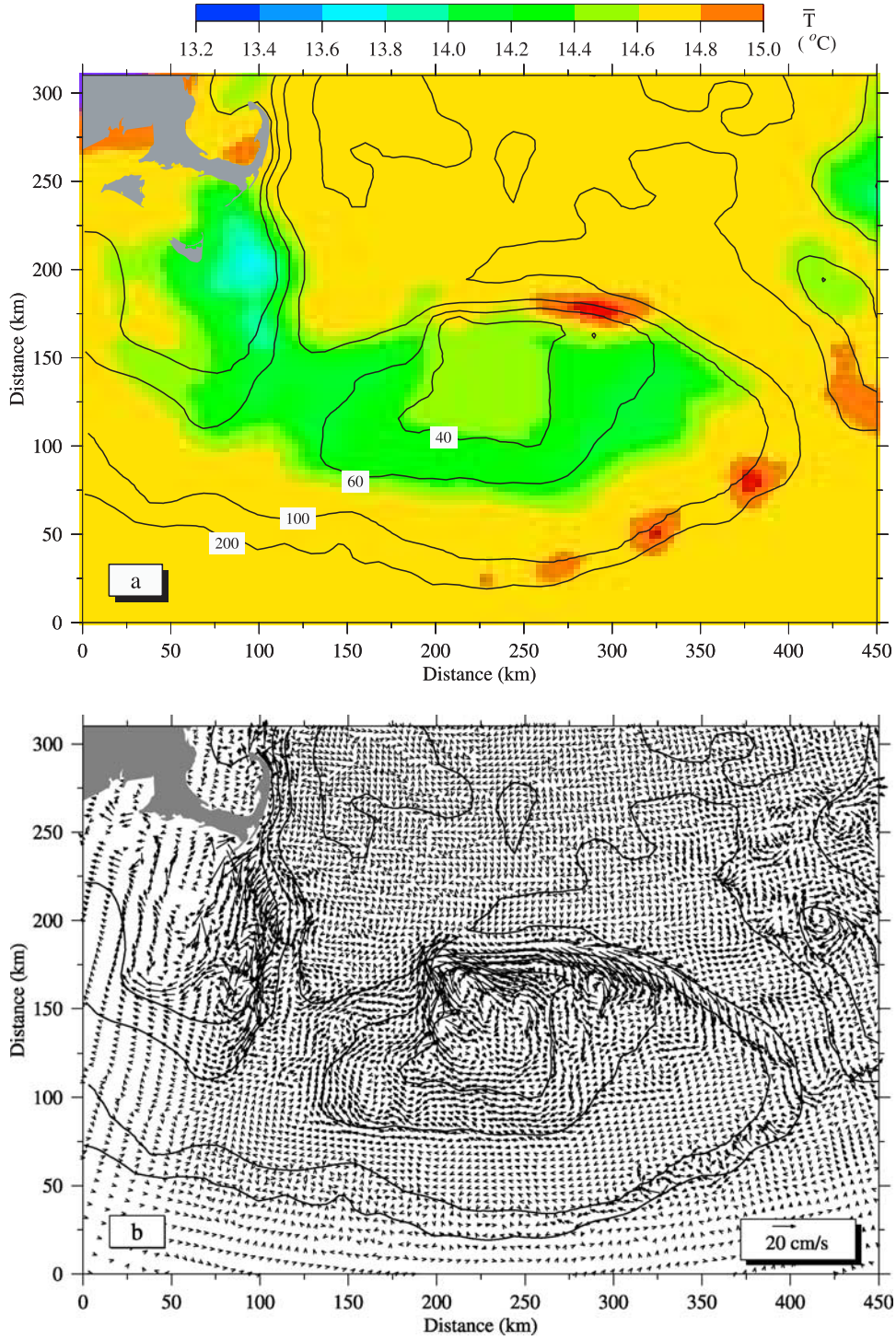

Figure 5. Tidally averaged (a) temperature and (b) residual current near the surface over Georges Bank, Nantucket Shoals, and Browns Bank for the case with only tidal forcing (Q_n = 0).

frequency warming trend of water within the mixed region is less sensitive to the different sets of shortwave attenuation lengths than in the stratified region. In the mixed region, tidal mixing is much stronger than the buoyancy input from heating, so the water always remains vertically well mixed no matter how the heat is input. The low-frequency warming tendency in this area depends only on the amplitude of the net surface heat flux at the surface and not on the vertical structure of the shortwave flux within the water column. In the stratified region, however, tidal mixing is too weak to transfer heat efficiently in the vertical, so the water temperature is strongly influenced by the vertical absorption of the shortwave flux.

[22] The model results also show that the diurnal variation of the near-surface water temperature depends on the vertical variation of the shortwave flux component. The

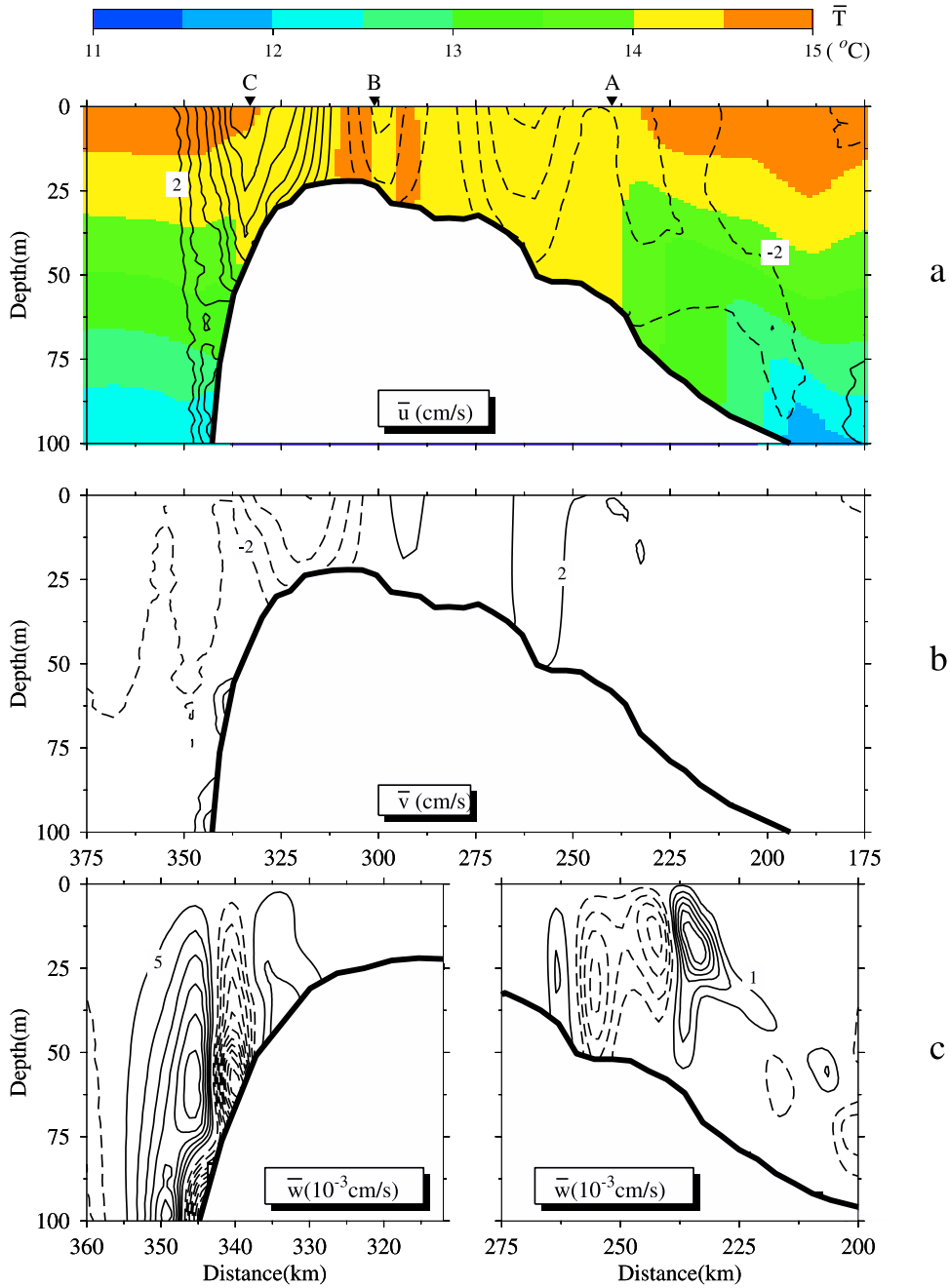

Figure 6. Cross-bank distributions of temperature ($\bar{T}$) (a) along-bank ($\bar{u}$) and (b) cross-bank ($\bar{v}$) currents, and (c) vertical current ($\bar{w}$) averaged over a tidal cycle on the section across Georges Bank shown in Figure 1. The contour interval is 2 cm/s for horizontal current components, 5×10^{-3} cm/s for positive vertical velocity and 10×10^{-3} cm/s for negative vertical velocity on the northern flank, and 1.0×10^{-3} cm/s for vertical velocity on the southern flank.

daily variation of the surface water temperature measured at the STI meteorological buoy in the stratified region of the southern flank in July–August 1995 (see Figure 1) had a range of 1° to 3°C during periods with little wind. Assuming that the observed daily temperature variation is a result of the diurnal cycle in the surface heat flux, the model, which ran with either a single attenuation length (case C) or two distinct sets of attenuation lengths for mixed and stratified waters (case D), underestimates the daily variation of the near-surface water temperature in the stratified region. When all the heat flux is absorbed in the top model layer, the model overestimates the daily variation in near-surface water in both stratified and mixed regions (case B).

[23] The net surface heat flux input into the model varies with a diurnal cycle. The daily averaged value of the net heat flux is about 365 W/m^2. For a given spatially uniform but time-varying surface heat flux (with inclusion of a downward shortwave flux), the model shows that surface water is heated much faster in the stratified region than in the mixed region. This spatial difference does not change

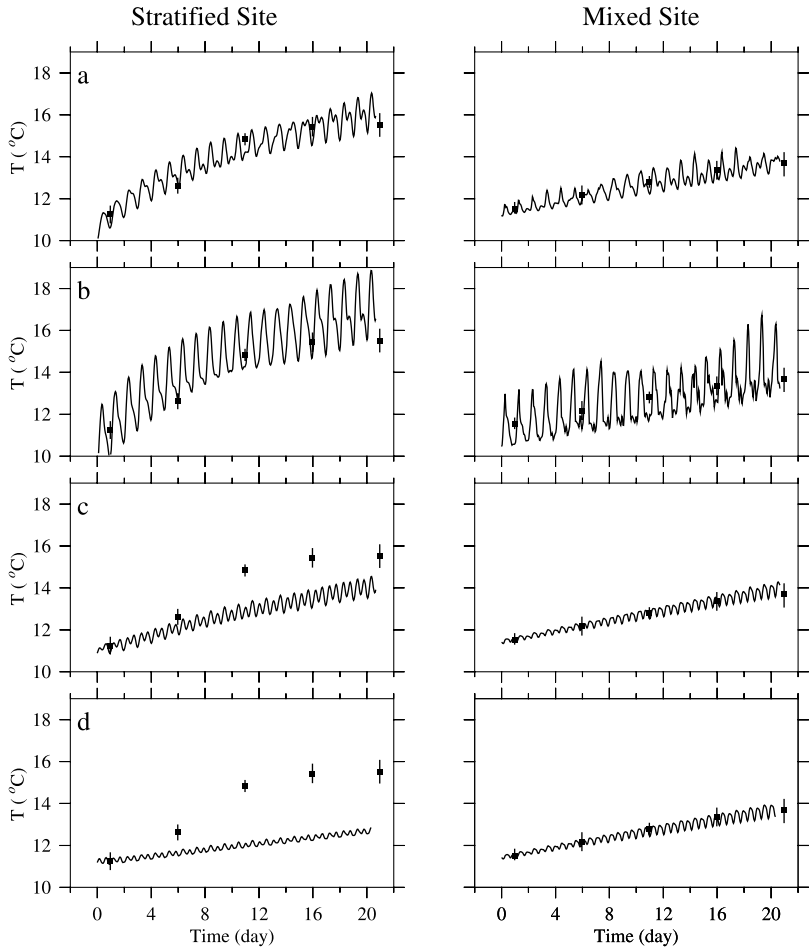

Figure 7. Comparison of model-predicted surface temperature (solid line) and satellite SST (solid square) at mixed and stratified sites (shown as solid squares in Figure 1) over Georges Bank for the four cases with different shortwave penetration parameters: (a) case A (our best parameters), (b) case B (surface heating only), (c) case C (deep penetration by a single shortwave component), and (d) case D (coastal parameters in mixed area, open ocean parameters for stratified waters). The satellite SST data were averaged daily with a record interval of 5 days from 21 June to 11 July 1995. The resulting SST values were averaged over 5 points around selected model grid points for the model-data comparison. The vertical line shown at each SST value indicates the deviation of the 5-point values used to compute the average.

the basic patterns of tidal mixing fronts over GB and adjacent coastal regions in the GOM. A relatively cold water band still exists within the frontal zone on the southern flank of GB between waters on top of the bank and stratified region (Figure 8a).

[24] Heating strengthens the tidal mixing front (Figures 8 and 9). The location of the front remains almost unchanged on the northern flank, but it moves gradually onto the bank on the southern flank as seasonal stratification develops. Correspondingly, the along-bank residual current increases to 30–35 cm/s on the northwestern flank, about 5–7 cm/s larger than that generated for the case with the only tidal forcing (Figure 8b). On the cross-bank section shown in Figure 9a, the along-bank current reaches 22 cm/s, which is ~6 cm/s larger than that shown in Figure 6. A relatively strong northeastward current appears on the eastern side of GSC, which flows along the 100-m isobath and joins the clockwise circulation gyre on the northeast flank of GB.

[25] The cross-bank secondary circulation is also modified after the surface heat flux is added (Figure 9). On both southern and northern flanks, heating significantly increases the near-surface, on-bank flow in the stratified region and thus considerably enhances the convergence at the tidal mixing front. On the northern flank, heating also causes an additional maximum core of upwelling near the surface, which seems to be directly linked to the intensification of the near-surface frontward convergence. Model-computed intensification of frontward convergence on both southern and northern flanks of GB is consistent with recent U.S. GLOBEC drifter measurements [*Limeburner and Beardsley*, 1996; *Churchill and Manning*, 1997; *Drinkwater and Loder*, 2001]. Trajectories of drifters tended to converge toward the frontal zone around GB during summer. This tendency may be due to the heating-intensified convergence flow near the front.

[26] It should be pointed out here that ignoring the downward shortwave flux in the case with only surface heating (case B) fails to capture the spatial distribution of the surface temperature on GB (Figure 10a). The observed summertime SST on GB is characterized by a relatively cold

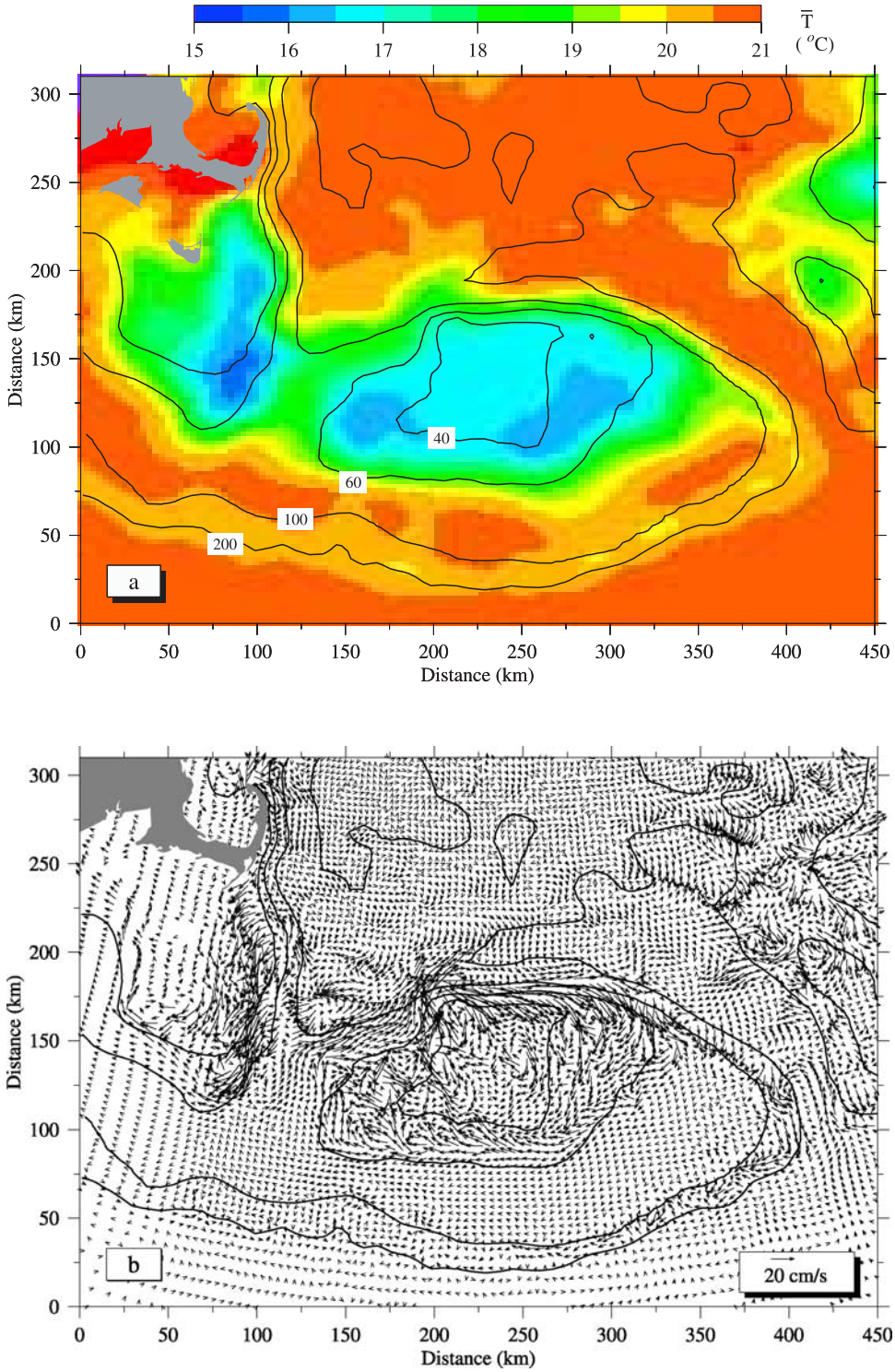

Figure 8. Distributions of near-surface (a) temperature and (b) current vectors averaged over two tidal cycles over Georges Bank and Nantucket Shoals on day 16 (counting from the starting time of heating) for case A (with our best estimates of the shortwave penetration parameters).

water band in the tidal mixing frontal zone on the southern flank, which separates the relatively less cool water on the crest from the warmer water in the stratified region. These features disappear in the near-surface water temperature pattern computed by the model for case B. In this case, vertical diffusion is a key physical process to transfer the heat downward. Since the vertically averaged magnitude of vertical diffusion decreases with the water depth on the bank, tidal mixing within the frontal zone is not large enough to mix the surface heat to the bottom as fast as that in the mixed region. For a given same heat flux at the surface a cold water band in the frontal zone no longer exists.

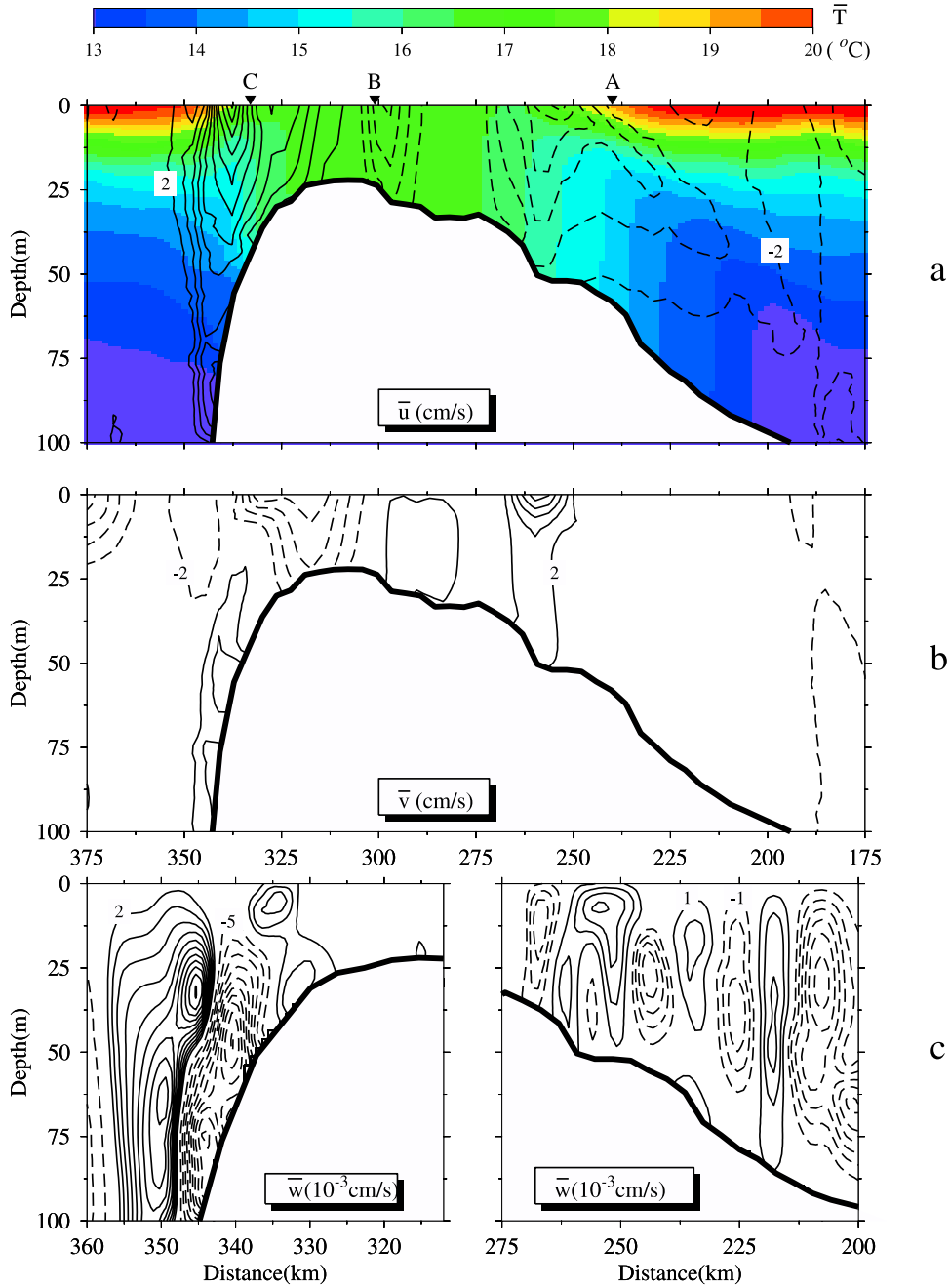

Figure 9. Cross-bank distribution of temperature ($\bar{T}$) (a) along-bank ($\bar{u}$) and (b) cross-bank ($\bar{v}$) currents, and (c) vertical current ($\bar{w}$) averaged over a tidal cycle on day 16 after heating is added using case A parameter values. The location of the section is shown in Figure 1. The contour interval is 2 cm/s for horizontal current components, 2×10^{-3} cm/s for positive vertical velocity and 5×10^{-3} cm/s for negative vertical velocity on the northern flank, and 1.0×10^{-3} cm/s for vertical velocity on the southern flank.

[27] In spite of the differences in the distribution of temperature the model-computed three-dimensional residual circulation patterns are very similar for the cases with and without inclusion of the downward shortwave flux (Figures 10, 11, and 12). The influence of attenuation lengths of the downward shortwave flux on the residual current is mainly in intensity and magnitude. For example, the surface-intensified, frontward convergence tends to weaken as the downward shortwave penetration in the stratified region becomes deeper (Figures 13 and 14).

3.3. Response of Tidal Flow to the Diurnal Variation of Heat Flux

[28] The response of tidal flow to the diurnal variation of the surface heat flux was examined for four cases with the starting time of heating at (case 1) ebb-flood transition, (case 2) maximum flood, (case 3) flood-ebb transition, and

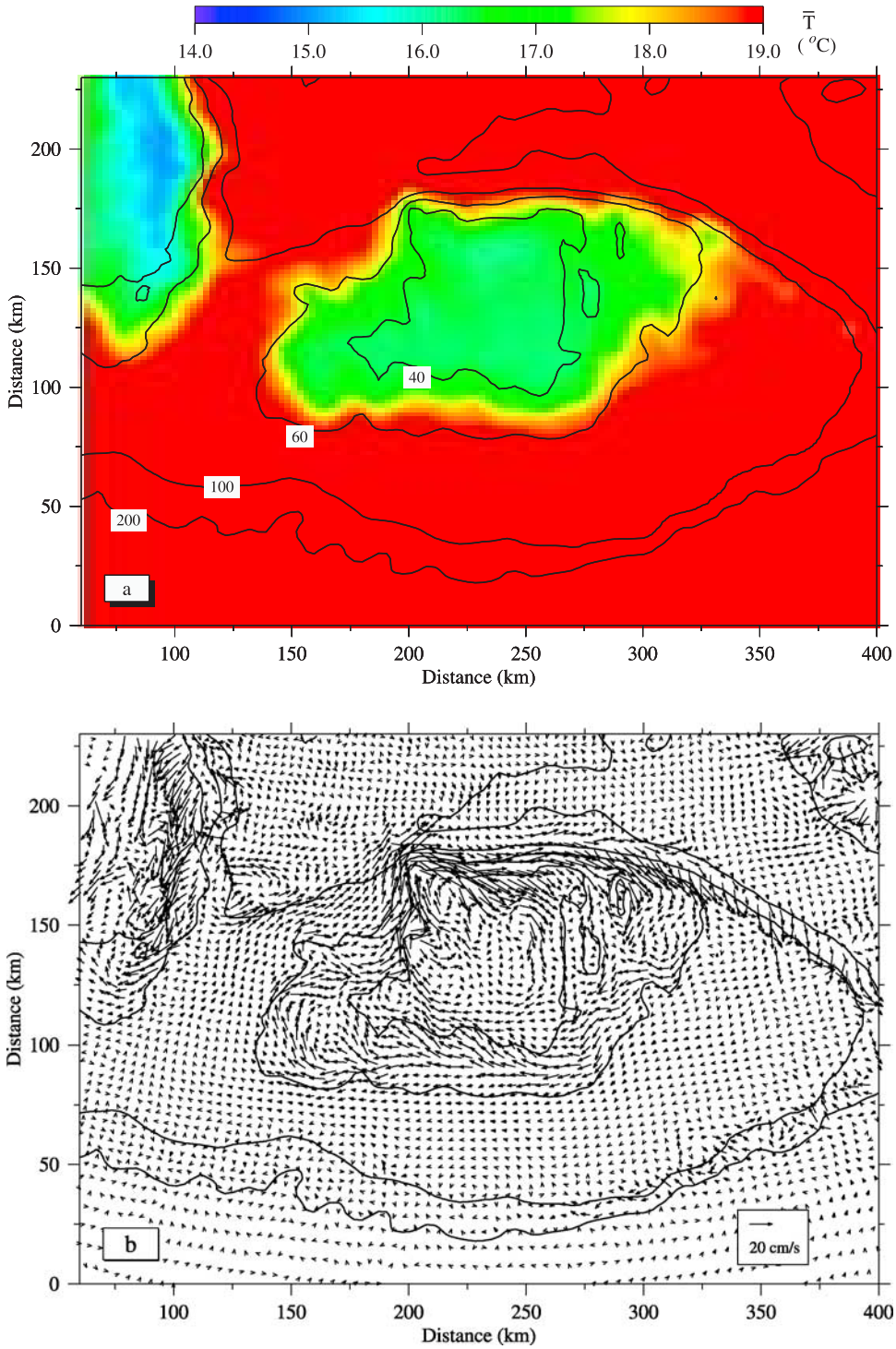

Figure 10. Distributions of near-surface (a) temperature and (b) current vectors averaged over two tidal cycles over Georges Bank on day 8 after heating was started using case B (surface heating only) parameters.

(case 4) maximum ebb (Figure 15). To identify the quantitative contribution of heating to the water current, we define the heat-induced current (Δu and $\Delta \upsilon$) as a difference between the model-computed currents for the cases with and without heating. The model results show that the response of tidal currents to the diurnal heat flux varies spatially across GB, and the basic structure of the heat-induced current is not significantly altered by the relative phase of heat flux to tidal currents. These features can be clearly seen at selected sites A–C described below.

[29] At site A (53-m isobath) on the stratified side of the tidal mixing front over the southern flank both along- and cross-bank tidal currents for all the cases exhibited some change in both phase and amplitude after heating is added (Figure 16, top plot). The resulting heat-induced current varies with a tidal cycle, with a maximum value of about 15

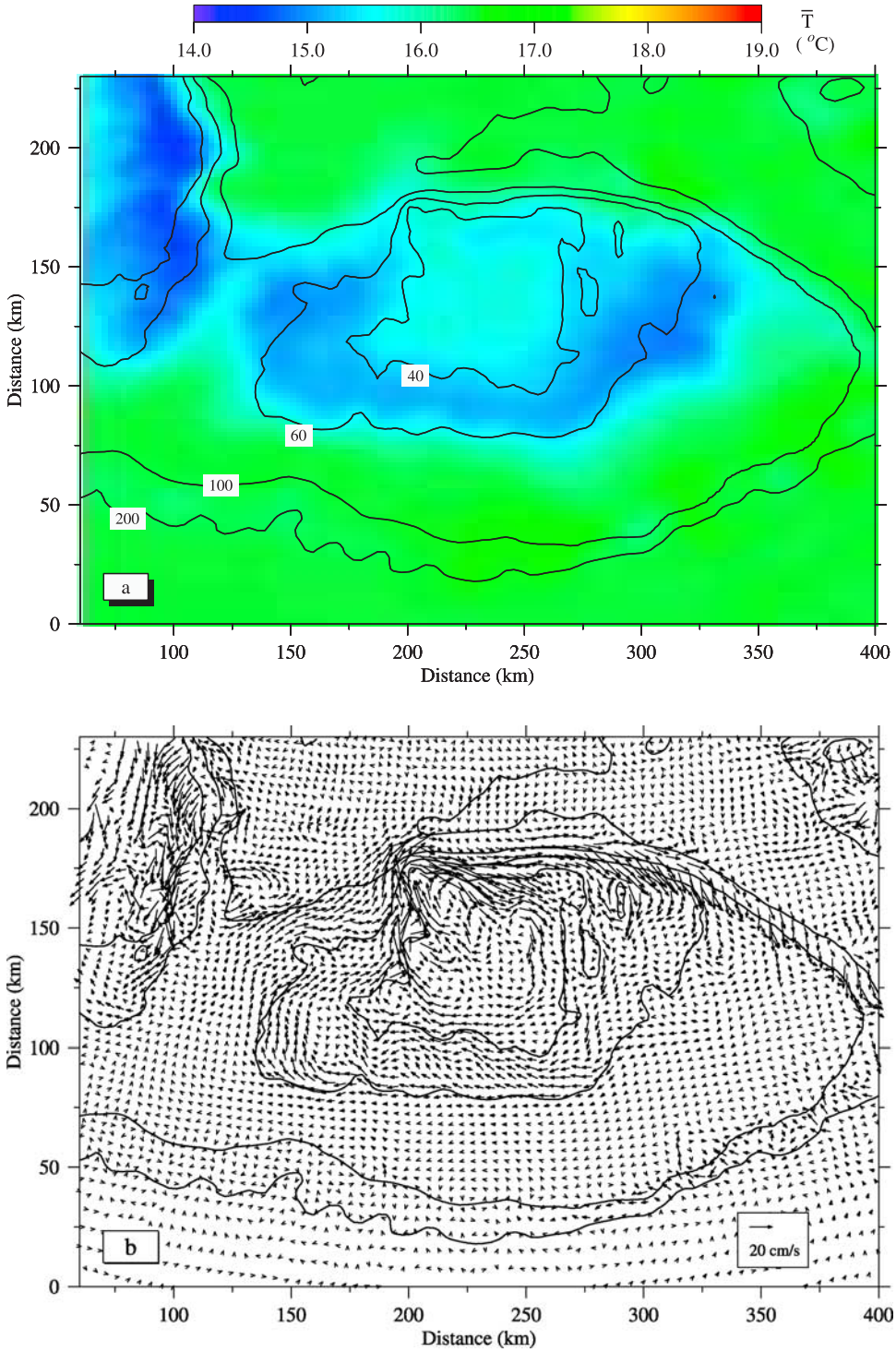

Figure 11. Distributions of near-surface (a) temperature and (b) current vectors averaged over two tidal cycles over Georges Bank on day 8 after heating was started using the case C ("deeper penetration") parameters.

to 20 cm/s occurring near the tidal current transition. Averaging over four tidal cycles produces a westward along-bank flow of about 4 to 6 cm/s and an on-bank flow of 1.7 to 2 cm/s (Figure 17, top plot).

[30] At site B (25-m isobath) on the crest of the bank where the water is vertically well mixed, the response of tidal currents to the heat flux is relatively weak and asymmetric over a tidal cycle (Figures 16 and 17, middle plot). The maximum current is 1.4 cm/s (eastward) in the along-bank direction and up to 0.9 cm/s (on bank) in the cross-bank direction (Figure 17, middle plot).

[31] At site C (50-m isobath) on the northern edge where the tidal mixing front is located, in the along-bank direction, heating generates a strong eastward current component of

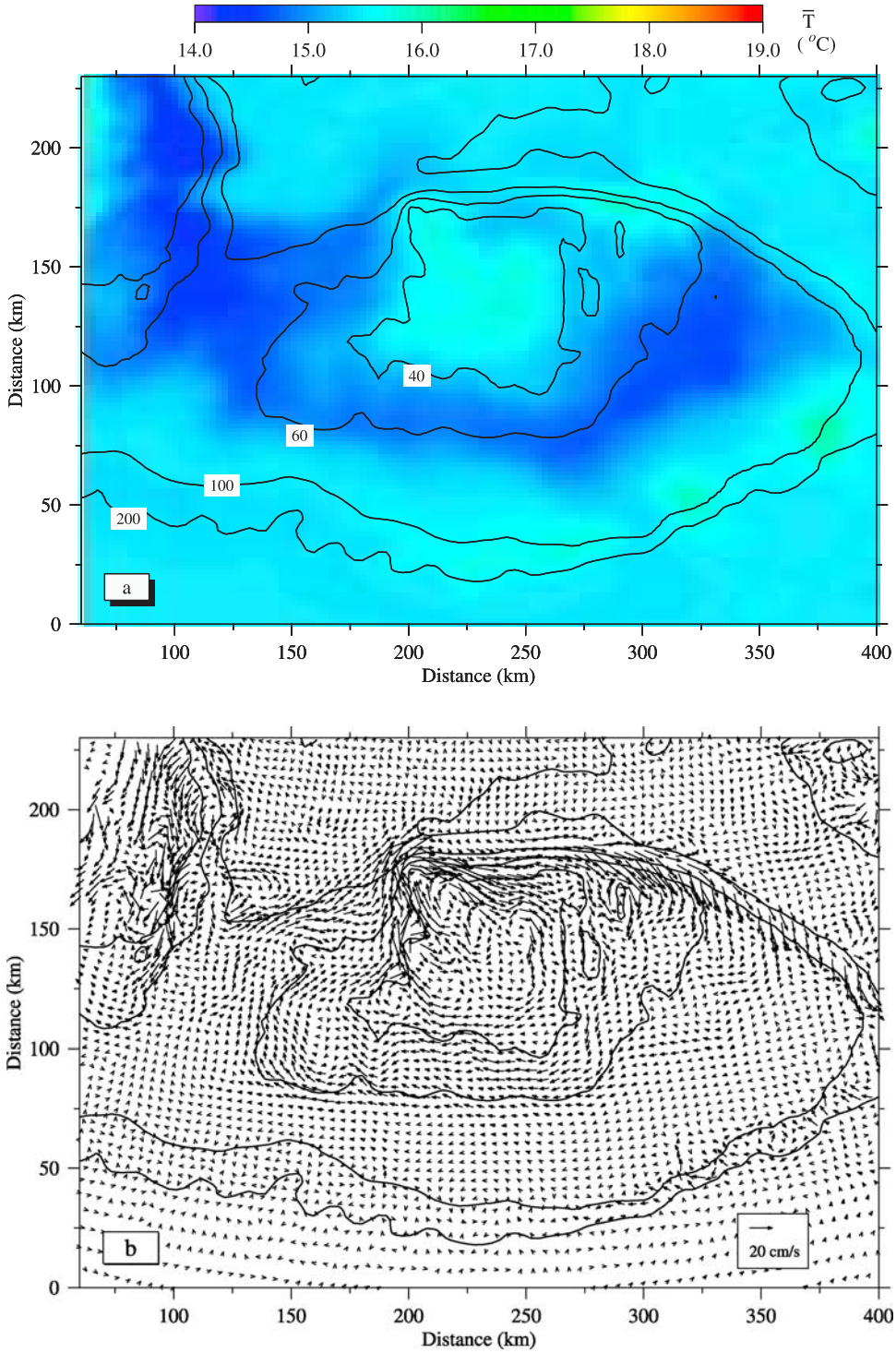

Figure 12. Distributions of near-surface (a) temperature and (b) current vectors averaged over two tidal cycles over Georges Bank on day 8 after heating was started using case D (coastal/open ocean) parameters.

up to about 30 cm/s around the eastward tidal current crest, while it has little influence on the tidal current around the westward tidal current trough (Figure 16, bottom plot). An eastward residual current, averaged over four tidal cycles, is about 5.7 to 6.2 cm/s (Figure 17, bottom plot). This flow directly contributes to an intensification of the residual jet current on the northern flank. In the cross-bank direction, heating tends to increase both off-bank and on-bank tidal currents, with a maximum value around the maximum on- and off-bank tidal flows (Figures 16 and 17, bottom plot). Heating produces a net weak off-bank residual current of about 0.6 to 1.5 cm/s near the surface, which coincides well with the location of the maximum upwelling on the northern flank (Figure 9). The physical mechanism causing the

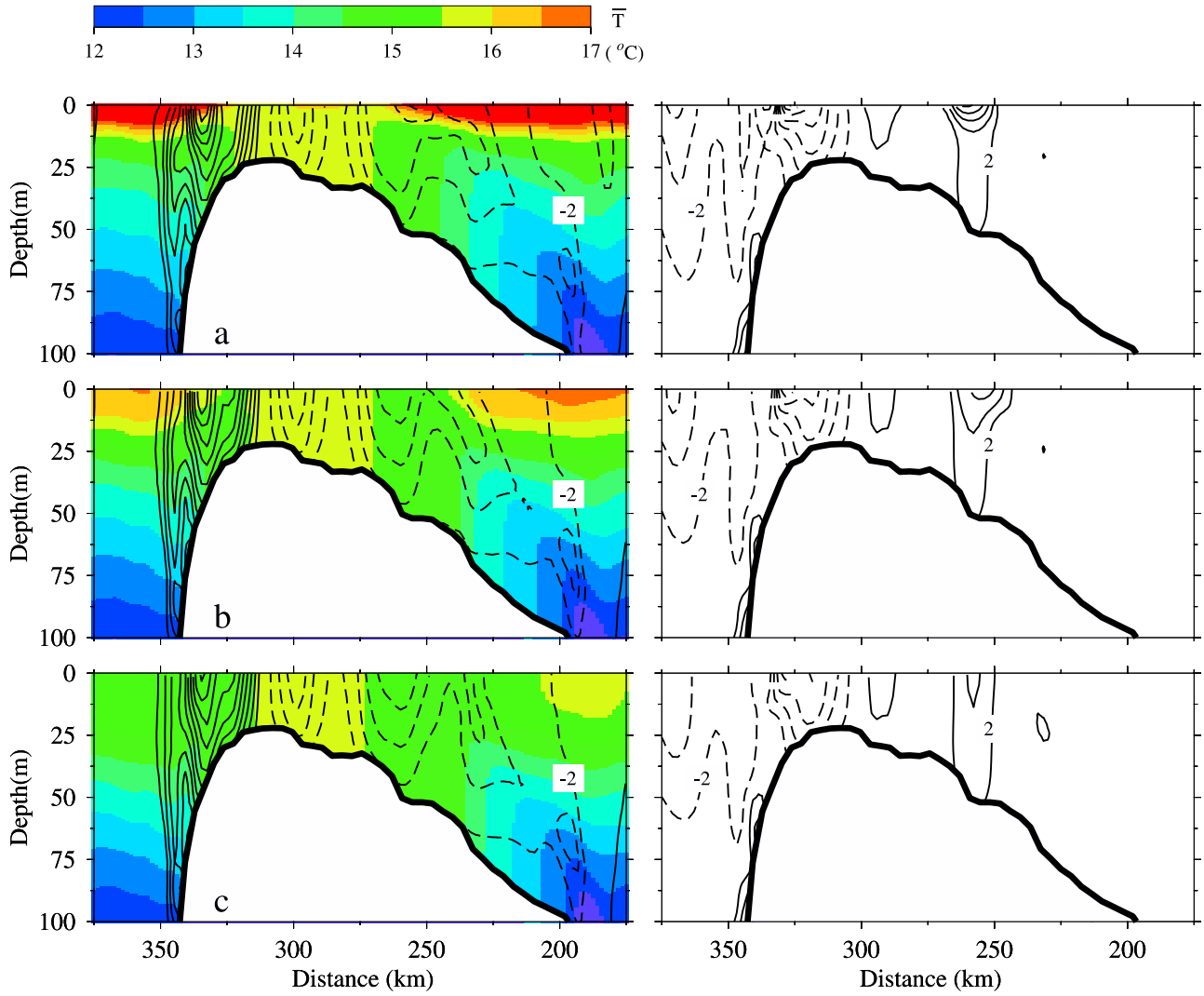

Figure 13. Cross-bank distributions of temperature ($\bar{T}$) and along-bank ($\bar{u}$) and cross-bank ($\bar{v}$) velocities averaged over two tidal cycles on day 8 after heating was started for (a) case B (surface heating only), (b) case C (deeper penetration), and (c) case D (coastal/open ocean) parameters. The location of the cross-bank section is shown in Figure 1. The contour interval for velocity is 2 cm/s.

phase-locked feature in the response of tidal currents to the diurnal heat flux on the northern flank is unclear. Since this feature only occurs at the northern edge of GB where a strong stratified tidal-induced eastward residual current jet is located, we believe that the steep bottom slope on the northern edge of GB plays an essential role in the strong asymmetric response of tidal currents to the heat flux during tidal cycles.

4. Discussion

[32] These model results show that summer surface heating tends to enhance the near-surface convergence near the tidal mixing front and intensify the clockwise residual current gyre around GB. For a given spatially uniform but time-varying heat flux the response of tidal currents differs across the bank. A phase-locked feature is found in the heat-induced current at the northern edge where the tidal mixing front is located. As a result, the eastward residual current jet is intensified at the front.

[33] One approach to quantify the contribution of the diurnal heat flux on the residual current is to examine the momentum balance for the cases with and without heating. In particular, we can compute all the terms in the momentum equations for each heating case and look at the differences to provide some understanding about the tidal and diurnal heat flux interactions. Using the symbol $\Delta(\ )$ to indicate the difference of a term in the momentum equations between two cases, the difference of the residual current due to heating can be determined from a steady state momentum balance as follows:

$$\Delta\hat{v} = \frac{1}{f}\left[\Delta\left(\overline{uu_x}\right) + \Delta\left(\overline{vu_y}\right) + \Delta\left(\overline{wu_z}\right) + \Delta\left(\overline{p_x}\right) + \Delta\left(\overline{g\zeta_x}\right) - \Delta\overline{\left(K_m u_z\right)_z}\right] \tag{4}$$

$$\Delta\hat{u} = \frac{1}{f}\left[\Delta\left(\overline{uv_x}\right) + \Delta\left(\overline{vv_y}\right) + \Delta\left(\overline{wv_z}\right) + \Delta\left(\overline{p_y}\right) + \Delta\left(\overline{g\zeta_y}\right) - \Delta\overline{\left(K_m v_z\right)_z}\right] \tag{5}$$

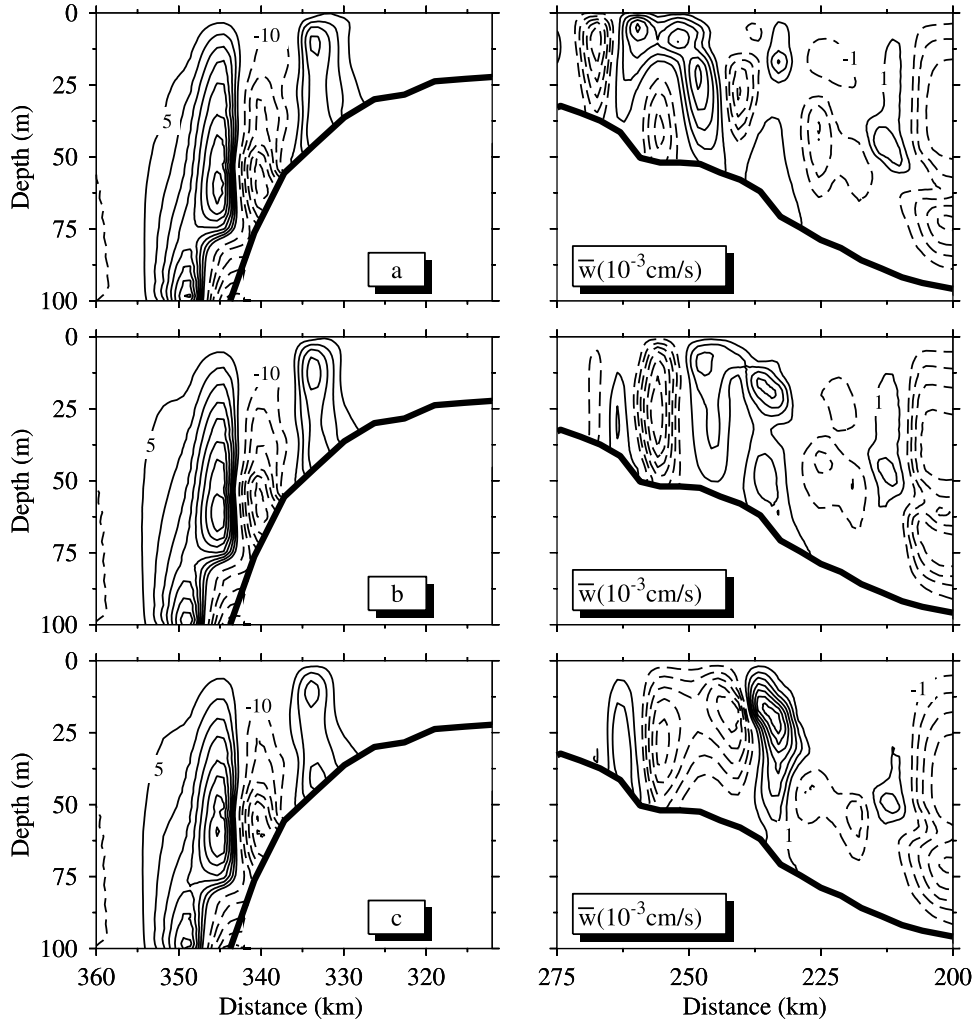

Figure 14. Cross-bank distribution of vertical velocity averaged over two tidal cycles on day 8 after heating was started using (a) case B (surface heating only), (b) case C (deeper penetration), and (c) case D (coastal/open ocean) parameters. The location of the cross-bank section is shown in Figure 1. The contour interval is 5×10^{-3} cm/s for positive vertical velocity and 10×10^{-3} cm/s for negative vertical velocity on the northern flank (left) and 1×10^{-3} cm/s on the southern flank (right).

where the overbar indicates a mean value averaged over four tidal cycles. Subscripts x, y, and z represent the along-bank, cross-bank, and vertical derivatives, respectively.

[34] Figure 18 shows the cross-frontal distribution of each term in the along-bank momentum equation (4) on the northern and southern flanks of GB. On the northern flank, Δu is primarily balanced by the cross-bank momentum flux $\Delta(\overline{vu}_y)/f$ against the along-bank surface pressure gradient $\Delta(g\overline{\zeta}_x)/f$ and vertical diffusion $[\Delta(\overline{K_m u_z})_z]/f$. The along-bank momentum flux $\Delta(\overline{uu}_x)/f$ is significant in the off-bank flow regime at the front, but it is negligible elsewhere. The along-bank baroclinic pressure gradient $\Delta\overline{p}_x/f$ and vertical advection $\Delta(\overline{wu}_z)$ are all too small to be taken into account. Similar results are found on the southern flank, where the cross-bank momentum flux $\Delta(\overline{vu}_y)/f$ directly contributes to an intensification of the near-surface, on-bank flow at the front and convergence in the stratified region.

[35] The momentum balance in the along-bank direction described above suggests that heating tends to enhance convergence and divergence on the stratified side and at the on-bank edge of the front, respectively. This enhancement is driven by a fully nonlinear process in which the cross-bank momentum flux of $\Delta(\overline{vu}_y)/f$ is dominant.

[36] Figure 19 shows the cross-frontal distribution of each term in the cross-bank momentum equation (5) on the northern flank. The significant positive value of Δu within the frontal zone corresponds to a peak of the cross-bank momentum flux of $\Delta(\overline{vv}_y)/f$. $\Delta(g\overline{\zeta}_y)$, $\Delta(\overline{uv}_x)/f$, and $[\Delta(\overline{K_m v_z})_z]/f$ change signs within the frontal zone, with smaller magnitudes than $\Delta(\overline{vv}_y)/f$. The cross-bank baroclinic pressure gradient $\Delta\overline{p}_y/f$ is one order of magnitude smaller thanall the other terms in the cross-bank momentum equation. This suggests that enhancement of the cross-bank density gradient caused by heating is generally smaller near the surface on the northern flank, so that it makes little contribution to an intensification of the eastward residual current jet within the frontal zone at the northern edge of GB. This finding is consistent with our previous modeling experiments on GB [*Chen et al.*, 1995a], in which we found that the stratified tidal rectification associated with the interaction

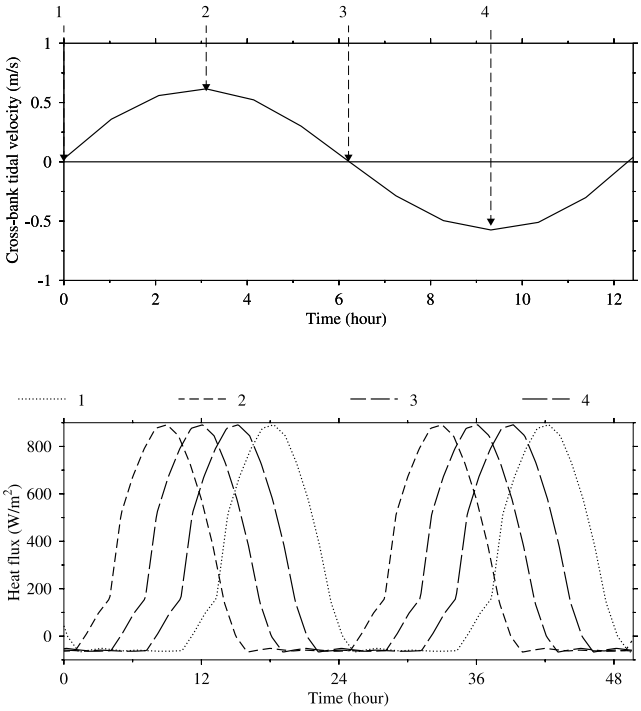

Figure 15. (top) Cross-bank near-surface tidal current on the southern flank of Georges Bank showing the four tidal phases: (1) transition to flood, (2) maximum flood, (3) transition to ebb, and (4) maximum ebb. (bottom) Model surface heat time series corresponding to having started at the four tidal phases shown in the top plot.

between barotropic and internal tidal currents is the dominant physical process that leads to the intensification of the eastward residual current jet on the northern flank of GB.

[37] The above analysis indicates that heating tends to enhance a convergence of the cross-isobath momentum flux on the stratified side of the front over an abrupt slope at the northern edge of GB. This convergence directly leads to an intensification of the eastward residual current jet in summer on the northern flank.

[38] This behavior is, to some extent, similar to the physical mechanism of tidal rectification described by *Loder* [1980]. In a tidal rectified system the cross-isobath momentum flux is balanced by bottom friction, while in a heating system this flux is balanced by the Coriolis force. Such a difference can be easily understood from the view of the physical mechanisms for tidal rectification and heating. Over GB, tidal mixing is a key element in barotropic tidal rectification. Since mixing starts at the bottom because of shear instability of tidal flow [*Chen and Beardsley*, 1995, 1998], bottom friction becomes a dominant term to balance the cross-isobath momentum flux of tidal flow. In a heating system, however, heat is input from the surface and plays a significant role in stabilizing the water column. Vertical diffusion reduces as vertical stratification develops. Therefore the heating-enhanced cross-isobath momentum flux is directly converted to the residual flow through a rotational adjustment.

[39] Our modeling findings are consistent with the recent drifter experiments conducted by *Limeburner and Beardsley* [1996] (LB), *Churchill and Manning* [1997] (CM), and *Drinkwater and Loder* [2001] (DL). In LB's experiments, satellite-tracked drifters with drogues centered at 5 and 50 m below the surface were launched during later winter and spring of 1988 and 1989 in the northern Great South Channel in the western GOM. The trajectories of these drifters showed a large seasonal change. They flowed clockwise around Georges Bank, showing a significant off-bank variation in winter but being trapped within the tidal mixing frontal zone in summer. CM's drifters were launched in the stratified region on the southern flank during late spring of 1995 and 1997. Trajectories of those drifters tended to converge toward the southern front at a speed of about 8 cm/s. Similar frontward convergence of drifters was also found in DL's drifter deployments made on the northern flank during the summer and autumn of 1988 and 1989. These observational features were reasonably reproduced in previous Lagrangian modeling experiments made by *Naimie et al.* [2001] and *Chen et al.* [2003]. Our current numerical experiments suggest that heating might directly contribute to the intensification of the frontward convergent flow in summer and also be one of the key reasons why the drifters are trapped within the tidal mixing frontal zone during early summer through autumn.

[40] *Edwards et al.* [2001] proposed that the phytoplankton-caused cross-frontal variation of light attenuation coefficient could lead to the cross-frontal density gradient for a given same surface heat flux. This density gradient could cause an along-front low-frequency current with a basic balance among the Coriolis force, baroclinic pressure gradient, and vertical diffusion. Unlike the physical process described by *Edwards et al.* [2001], in our numerical experiments the surface heat flux is spatially uniform, and light attenuation coefficients are constant. So, if only heat flux is considered, there is no physical mechanism that could cause the cross-isobath density (thus pressure) gradient in our case. Two physical processes could cause the intensification of the front under spatially uniform heating conditions on GB. The first is vertical mixing, and the second is advection. Mixing is stronger in the mixed region than in the stratified region. When a uniform heat flux is applied at the surface, heat would concentrate in the upper 10 m in the stratified region, but it would be mixed throughout the entire water column in the mixed region (about 40 m on the top of GB). When heating is added into the model, strong tidal currents could redistribute heat into the deeper region over a vertical tidal advection scale of 60–100 m on the northern flank. In our experiments, however, the model results show that the tidal cycle-averaged, cross-isobath baroclinic pressure gradient is one order of magnitude smaller than the cross-isobath advection term in considering the contribution to heating-induced intensification of the eastward current. This suggests that the heating-induced increase of the cross-isobath density gradient is not the dominant process causing intensification of the current jet on the northern flank.

[41] On the other hand, in our current experiments the initial temperature field is linear in the vertical. The front predicted by the model is a pure tidal mixing front with no inclusion of the lateral buoyancy input. This differs from the front described in previous studies by *Loder and Wright* [1985] and *Naimie et al.* [1994]. In their experiments the

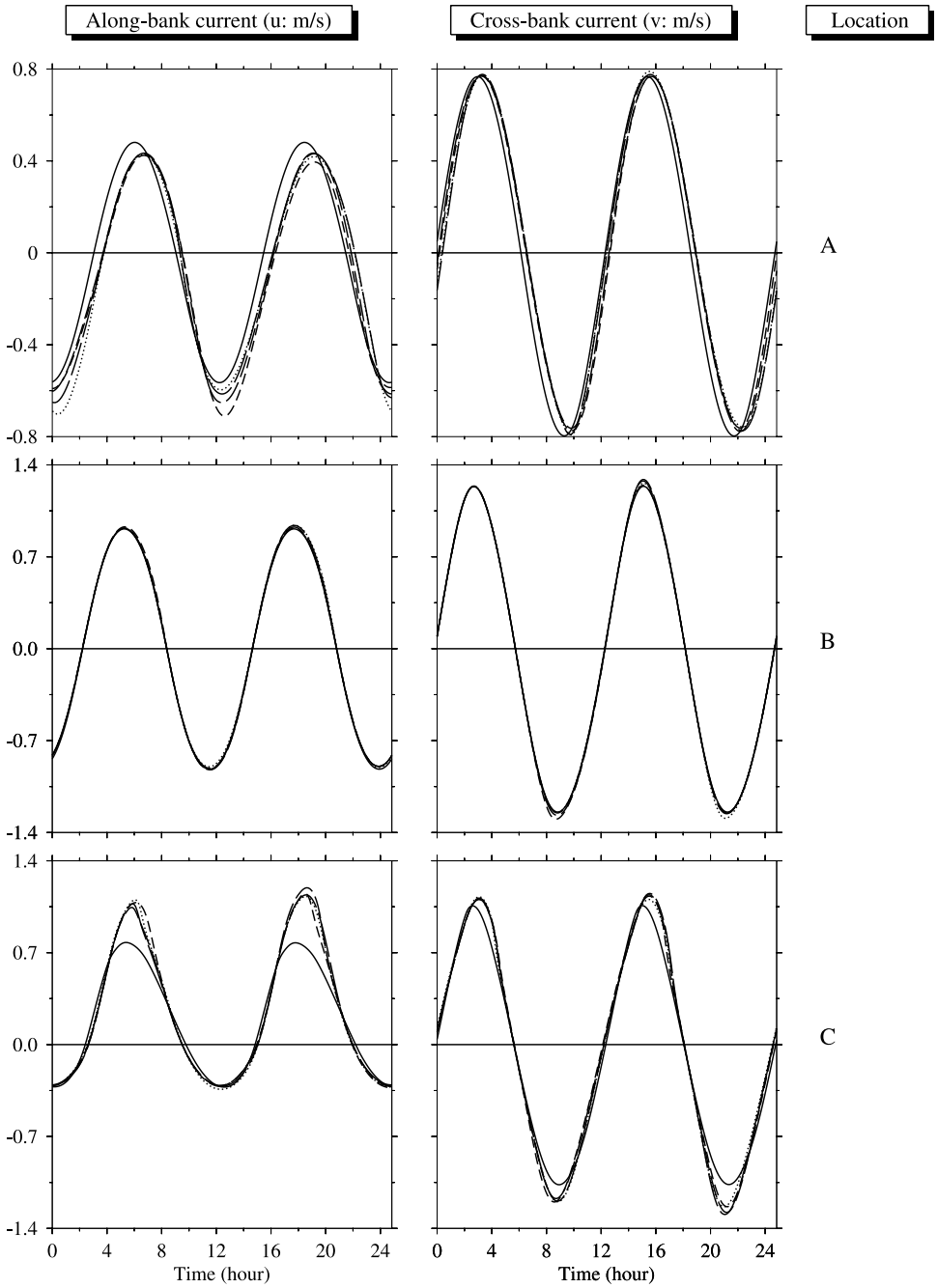

Figure 16. Time series of near-surface along-bank (u) and cross-bank (v) currents at sites A, B, and C over two tidal cycles on day 16 for the four different heating time series shown in Figure 15. Types of lines used in Figure 16 for the four cases are the same as those shown in Figure 15. The model was run using the case A parameters.

initial field featured a density front. Therefore the frontal system described in their papers is driven by combined buoyancy and tidal forcing. Determining whether or not spatially uniform heating could contribute to the cross-isobath baroclinic pressure gradient within the tidal- and density-induced front on the northern flank of GB requires additional validation.

[42] Our previous studies suggest that the hydraulic jump created by the strong tidal current over the northern flank of GB is an important physical process in the dynamics of this region. This hydraulic jump could cause strong internal mixing during the off-bank tidal flow that would contribute to the redistribution of heat. Although it remains unclear how heating could increase the cross-isobath divergence and convergence, we believe that nonlinear processes (including this hydraulic jump) are potential contributors.

5. Summary

[43] The influence of the diurnal surface heat flux on summer stratification and residual circulation over GB is

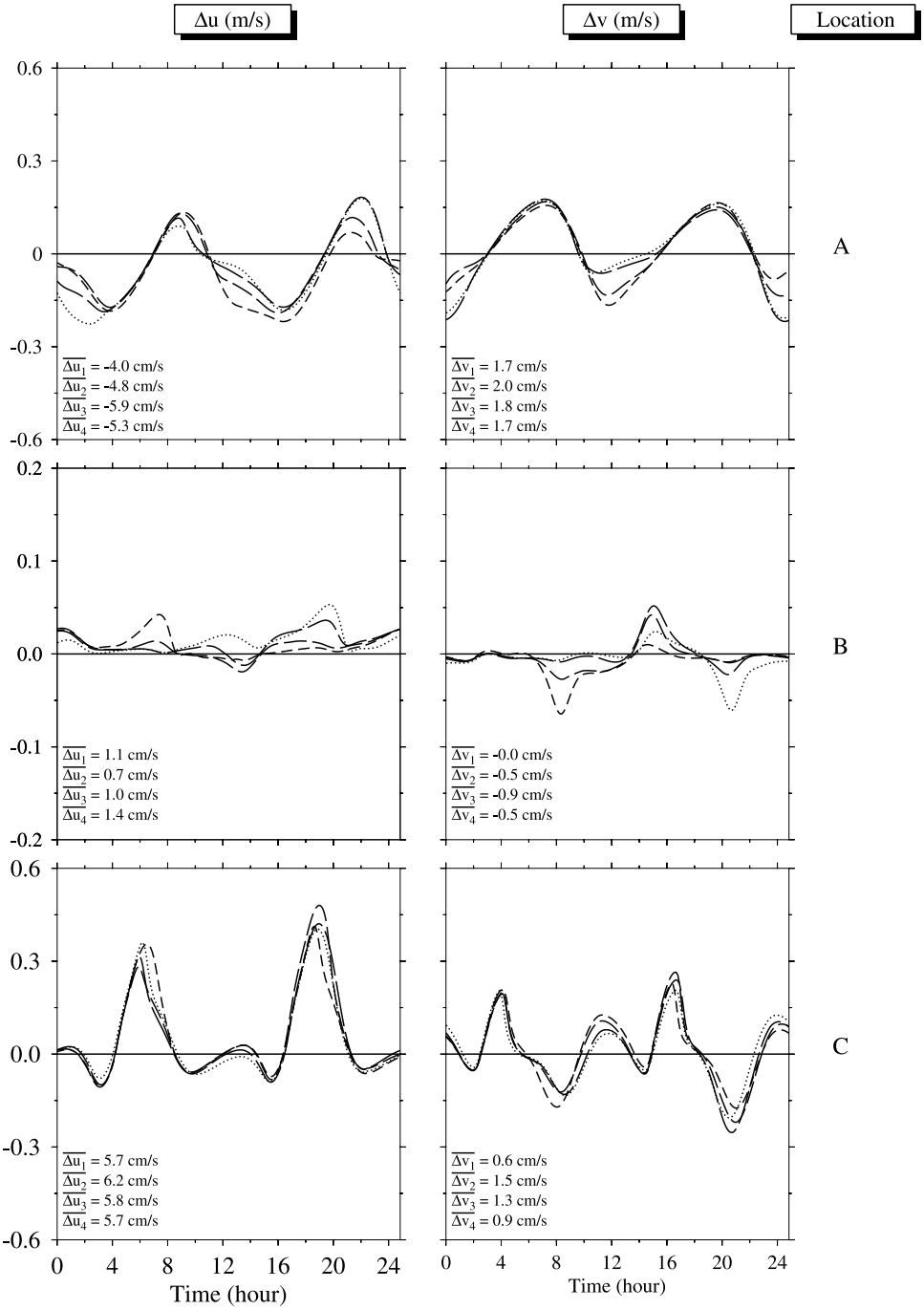

Figure 17. Time series of the difference of along-bank and cross-bank velocities at site A, B, and C between the four heating cases shown in Figure 15 and the model solution with only tidal forcing and without surface heating. Locations of sites A–C are shown at the top of Figure 9. The values in the lower left part of each plot are the differences of the velocity averaged over four tidal cycles, and subscripts 1–4 indicate the case numbers.

examined using a three-dimensional primitive equation numerical circulation model developed originally by *Blumberg and Mellor* [1987]. For a given spatially uniform and time-varying heat flux the model results show that the surface water is heated much faster on the southern flank than on the northern flank and much faster in the stratified region than in the mixed region. As a result, the location of the tidal mixing front gradually shifts on bank on the southern flank during the period of heating, but it remains almost unchanged on the northern flank. Heating tends to enhance the frontward convergent flow and leads to a significant intensification of the tidal mixing front. The model-predicted frontward convergence is consistent with recent drifter trajectories measured over

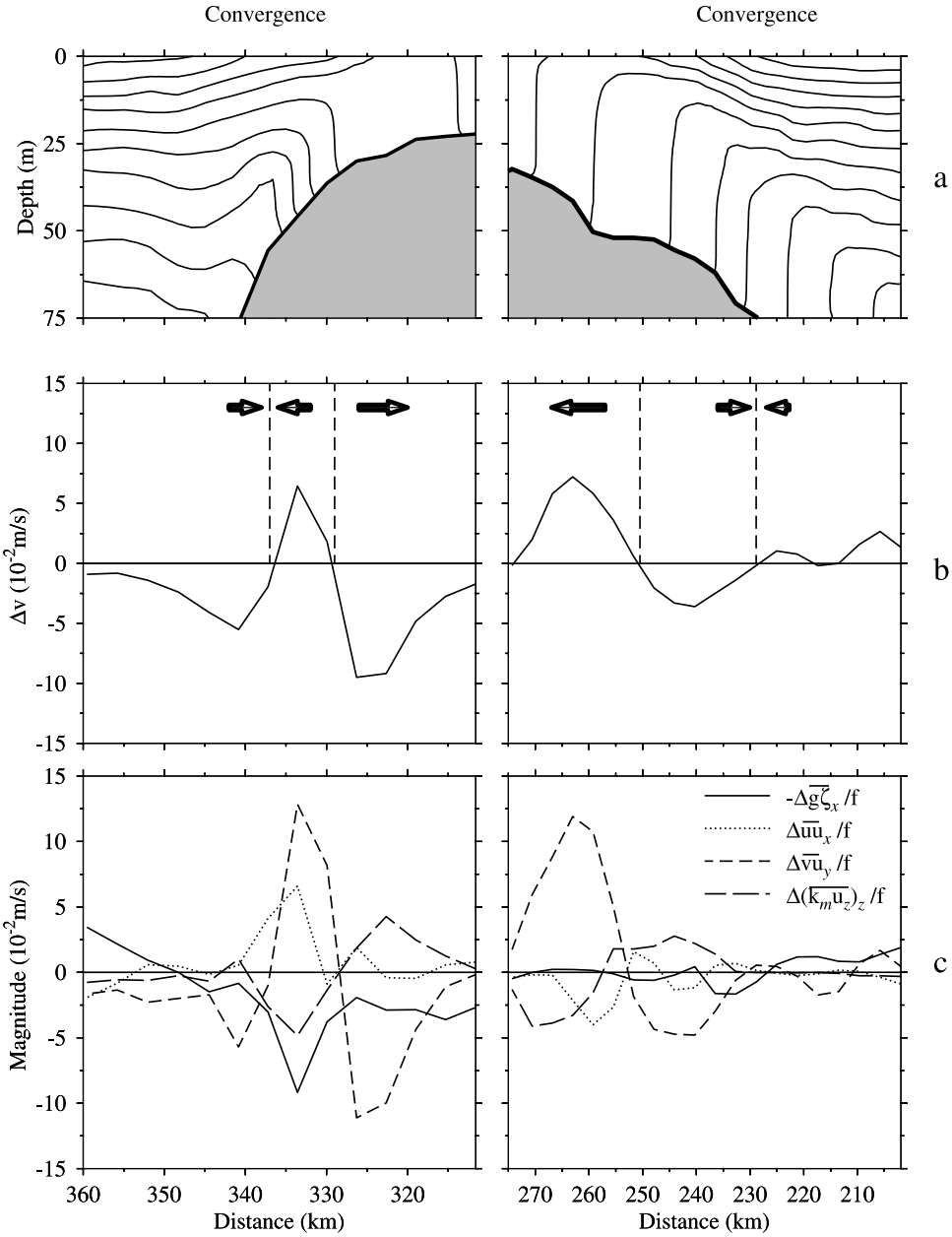

Figure 18. Cross-front distributions of (a) temperature, (b) the difference of cross-bank velocity for the cases with and without heating, and (c) the differences of terms in the along-bank momentum equation for the cases with and without heating on the southern (right) and northern (left) flanks of Georges Bank. The model results shown in Figure 18 were obtained using the case A parameters. Dashed vertical lines shown in the middle plot are the boundaries of the tidal mixing front.

GB. This heating-enhanced frontward convergence of the tidal flow is probably one of the key reasons why drifters tend to be trapped within the tidal mixing frontal zone in summer.

[44] Response of the tidal currents to the diurnal heat flux also exhibits an asymmetry across GB. On the southern flank the tidal currents respond periodically with diurnal heating, with a small modification of residual currents. On the northern flank, however, it is phase-locked around the crest of the eastward current, which directly contributes to an intensification of the current jet on the northern flank. Diagnostic analysis suggests that the heat-intensified, near-surface eastward residual current jet on the northern flank is mainly driven by the heat-enhanced convergence of the cross-isobath momentum flux of the tidal currents.

[45] These numerical experiments also indicate that the seasonal warming tendency of the surface water critically depends on the shortwave penetration parameters (R, a, and b) in the stratified region but not in the mixed region. On the basis of the comparison of the trends between model-predicted surface temperature and satellite-derived

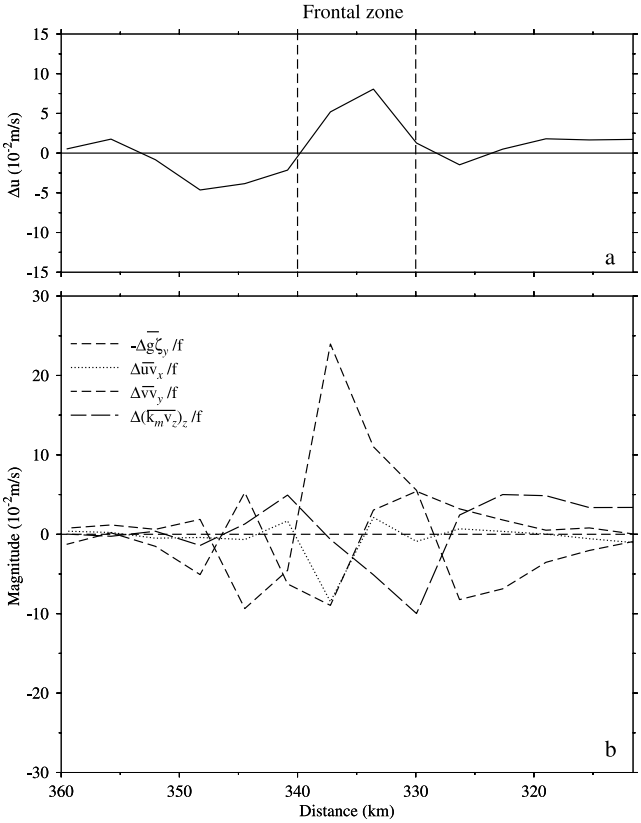

Figure 19. Cross-front distributions of (a) the difference of the cross-bank velocity and (b) the differences of terms in the cross-bank momentum equation for cases with and without heating on the northern flank of GB. These model results were obtained using case A parameters. Dashed vertical lines shown in the top plot are the boundaries of the tidal mixing front on the northern flank.

SST data in both mixed and stratified regions over GB, the downward shortwave penetration parameters for case A gave more realistic model temperature fields that those obtained using the parameters of cases B–D. Until additional data on shortwave penetration taken on or near GB become available, we recommend using case A parameters for future numerical circulation studies on GB.

[46] It should be noted here that these idealized model studies did not include explicit air-sea exchange. The sensible and latent heat flux components were used to compute the model net diurnal flux at the surface but were not included in the model surface boundary conditions. Therefore there was no explicit way for the model ocean to gain or lose heat through air-sea exchange. For the spatially uniform, time-varying heat flux used here with case A parameters, the model near-surface water temperature increases rapidly in the first 20 model days before slowing slightly. It is unclear if a steady state solution exists in this idealized case or how long it would take to reach. Fortunately, the actual surface heat flux has a large seasonal cycle, so that long (several months or more) model solutions can be run without fear of thermal runaway. For longer model simulations it may be necessary to include explicitly air-sea processes that allow feedback from the ocean to the atmosphere.

Appendix A: Estimation of *b* Using in Situ PAR

[47] Estimation of b was made using in situ profiles of photosynthetic active radiation (PAR) collected on GB during May-June 1995 on the R/V *Endeavor* (EN267A). At each PAR station, surface PAR data were measured with a Biospherical Instruments deck unit (PUV-510), while profile data were collected using a Biospherical Instruments underwater unit (PUV-500). These units measured radiation over the 400 to 700-nm-wavelength bands with an upward facing cosine sensor. All profiles were taken using the starboard side J frame, and the ship was turned such that the Sun was shining on the starboard side and as close to mid ship as possible whenever sea conditions allowed. During this cruise, three profiles were obtained within the well-mixed region on the southern flank, and seven profiles were obtained within the stratified area on the southern flank. The PAR downcast data from all ten stations, normalized by the simultaneous surface PAR data, are shown in Figure A1. In this semilog format a straight line indicates simple exponential decay. While most stations exhibited approximately linear behavior beneath 10 m, both in the well-mixed and stratified areas, several profiles were curved, suggesting layers with different optical absorption. Overall, the variation of normalized PAR within the two areas was as large as that between the areas, suggesting that optical clarity can vary on short horizontal scales within both areas. With this limited data set we could not distinguish between the stratified and well-mixed areas, so that

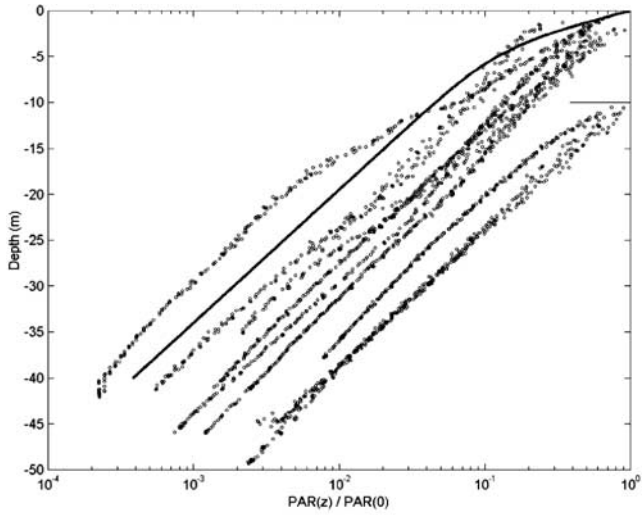

Figure A1. Vertical profiles of photosynthetic active radiation (PAR) plotted as a function of depth, normalized by the incident surface PAR. The solid profile was made using the case A parameters: $R = 0.78$, $a = 1.4$ m, and $b = 6.3$ m. The normalized profiles of PAR have been split into two groups of stations, the first located in the stratified zone along the southern flank and the second in the well-mixed zone over the crest of GB (these latter profiles have been shifted downward by 10 m to separate the two groups).

the value of b used in the numerical model represented an average over all ten profiles shown in Figure A1.

[48] **Acknowledgments.** This research was supported by the U.S. GLOBEC Northwest Atlantic/Georges Bank program through NOAA grants NA56RG0487, NA960P003, and NA960P005 to C. Chen, NSF grants OCE 96-32357, OCE 98-06379, and OCE 02-27679 to R. Beardsley, and NOAA grant NA76GP0176 to Peter Franks. This is U.S. GLOBEC contribution number 411.

References

Beardsley, R. C., S. J. Lentz, R. A. Weller, R. Limeburner, J. D. Irish, and J. B. Edson, Surface forcing on the southern flank of Georges Bank, February–August 1995, *J. Geophys. Res.*, *108*(C11), 8007, doi:10.1029/2002JC001359, 2003.

Blumberg, A. F., and G. L. Mellor, A description of a three-dimensional coastal ocean circulation model, in *Three-Dimensional Coastal Models*, *Coastal Estuarine Sci.*, vol. 4, edited by N. Heaps, pp. 1–16, AGU, Washington, D. C., 1987.

Brink, K. H., R. Limeburner, and R. C. Beardsley, Properties of flow and pressure over Georges Bank as observed with near-surface drifters, *J. Geophys. Res.*, *108*(C11), 8001, doi:10.1029/2001JC001019, 2003.

Brooks, D. A., The influence of warm-core rings on slope water entering the Gulf of Maine, *J. Geophys. Res.*, *92*, 8183–8196, 1987.

Casulli, V., Semi-implicit finite-difference methods for the two-dimensional shallow water equations, *J. Comput. Phys.*, *86*, 56–74, 1990.

Chen, C., Variability of currents in Great South Channel and over Georges Bank, Ph.D. thesis, 283 pp., Mass. Inst. of Technol./Woods Hole Oceanogr. Inst. Joint Program, Cambridge, 1992.

Chen, C., and R. C. Beardsley, A numerical study of stratified tidal rectification over finite-amplitude banks. part I: Symmetric bank, *J. Phys. Oceanogr.*, *25*(9), 2090–2110, 1995.

Chen, C., and R. C. Beardsley, Tidal mixing over a finite amplitude asymmetric bank: A model study with application to Georges Bank, *J. Mar. Res.*, *56*, 1163–1201, 1998.

Chen, C., R. C. Beardsley, and R. Limeburner, A numerical study of stratified tidal rectification over finite-amplitude banks. part II: Georges Bank, *J. Phys. Oceanogr.*, *25*(9), 2111–2128, 1995a.

Chen, C., R. C. Beardsley, and R. Limeburner, Variability of water properties in late spring in the northern Great South Channel, *Cont. Shelf Res.*, *15*, 415–431, 1995b.

Chen, C., R. C. Beardsley, and P. J. S. Franks, A 3-D prognostic numerical model study of the Georges Bank ecosystem. part I: Physical model, *Deep Sea Res., Part II*, *48*, 419–456, 2001.

Chen, C., Q. Xu, R. C. Beardsley, and P. J. S. Franks, Model study of the cross-frontal water exchange on Georges Bank: A three-dimensional Lagrangian experiment, *J. Geophys. Res.*, *108*(C5), 3142, doi:10.1029/2000JC000390, 2003.

Churchill, J. H., and J. P. Manning, Horizontal convergence and dispersion over the southern flank of Georges Bank, paper presented at ICES 1997 Annual Science Conference, Int. Counc. for the Explor. of the Sea, Baltimore, Md., 25–30 Sept. 1997.

Drinkwater, K. F., and J. W. Loder, Near-surface horizontal convergence and dispersion near the tidal-mixing front on northeastern Georges Bank, *Deep Sea Res., Part I*, *48*, 311–340, 2001.

Edwards, A. M., T. Platt, and D. G. Wright, Biologically induced circulation at fronts, *J. Geophys. Res.*, *106*, 7081–7095, 2001.

Egbert, G. D., A. F. Bennett, and M. G. G. Foreman, TOPEX/POSEIDON tides estimated using a global inverse model, *J. Geophys. Res.*, *99*, 24,821–24,852, 1994.

Galperin, B., L. H. Kantha, S. Hassid, and A. Rosati, A quasi-equilibrium turbulent energy model for geophysical flows, *J. Atmos. Sci.*, *45*, 55–62, 1988.

Garfield, N., and D. L. Evans, Shelf water entrainment by Gulf Stream warm-core rings, *J. Geophys. Res.*, *92*, 13,003–13,012, 1987.

Kraus, E. B., *Atmosphere-Ocean Interaction*, 275 pp., Clarendon, Oxford, U.K., 1972.

Lentz, S. J., R. C. Beardsley, J. D. Irish, J. Manning, P. C. Smith, and R. A. Weller, Temperature and salt balance on Georges Bank February–August 1995, *J. Geophys. Res.*, *108*(C11), 8006, doi:10.1029/2001JC001220, 2003.

Limeburner, R., and R. C. Beardsley, Near-surface recirculation over Georges Bank, *Deep Sea Res., Part II*, *43*, 1547–1574, 1996.

Loder, J. W., Topographic rectification of tidal current on the sides of Georges Bank, *J. Phys. Oceanogr.*, *10*, 1399–1416, 1980.

Loder, J. W., and D. G. Wright, Tidal rectification and front circulation on the sides of Georges Bank, *J. Mar. Res.*, *43*, 581–604, 1985.

Mellor, G. L., and T. Yamada, A hierarchy of turbulence closure models for planetary boundary layers, *J. Atmos. Sci.*, *33*, 1791–1806, 1974.

Mellor, G. L., and T. Yamada, Development of a turbulence closure model for geophysical fluid problems, *Rev. Geophys.*, *20*, 851–875, 1982.

Mountain, D. G., G. A. Trout, and R. C. Beardsley, Surface heat flux in the Gulf of Maine, *Deep Sea Res., Part II*, *43*, 1533–1546, 1996.

Naimie, C. E., Georges Bank residual circulation during weak and strong stratification periods—Prognostic numerical model results, *J. Geophys. Res.*, *101*, 6469–6486, 1996.

Naimie, C. E., J. Loder, and D. Lynch, Seasonal variation of the 3-D residual circulation on Georges Bank, *J. Geophys. Res.*, *99*, 15,967–15,989, 1994.

Naimie, C. E., R. Limeburner, C. G. Hannah, and R. C. Beardsley, On the geographic and seasonal patterns of the near-surface circulation on Georges Bank—From real and simulated drifters, *Deep Sea Res., Part II*, *48*, 501–518, 2001.

Paulson, C. A., and J. J. Simpson, Irradiance measurements in the upper ocean, *J. Phys. Oceanogr.*, *7*, 952–956, 1977.

Smith, P. C., The mean seasonal circulation off southwest Nova Scotia, *J. Phys. Oceanogr.*, *13*, 1034–1054, 1983.

Smith, P. C., Seasonal and interannual variability of current, temperature and salinity off southwest Nova Scotia, *Can. J. Fish. Aquat. Sci.*, *46*, 4–20, 1989.

Simpson, J. J., and T. D. Dickey, The relationship between downward irradiance and upper ocean structure, *J. Phys. Oceanogr.*, *11*, 309–323, 1981a.

Simpson, J. J., and T. D. Dickey, Alternative parameterizations of downward irradiance and their dynamical significance, *J. Phys. Oceanogr.*, *11*, 876–882, 1981b.

R. C. Beardsley, Department of Physical Oceanography, Woods Hole Oceanographic Institution, Woods Hole, MA 02543, USA.

C. Chen, School for Marine Science and Technology, University of Massachusetts Dartmouth, New Bedford, MA 02742, USA. (c1chen@umassd.edu)

P. J. S. Franks, Integrative Oceanography Division, Scripps Institution of Oceanography, University of California, San Diego, La Jolla, CA 92093-0281, USA.

K. Van Keuren, Department of Biology, Woods Hole Oceanographic Institution, Woods Hole, MA 02543, USA.